Cancer Cell
Article

Hippo-Independent Activation of YAP by the *GNAQ* Uveal Melanoma Oncogene through a Trio-Regulated Rho GTPase Signaling Circuitry

Xiaodong Feng,[1,2] Maria Sol Degese,[1] Ramiro Iglesias-Bartolome,[1] Jose P. Vaque,[1] Alfredo A. Molinolo,[1] Murilo Rodrigues,[3] M. Raza Zaidi,[4] Bruce R. Ksander,[5] Glenn Merlino,[6] Akrit Sodhi,[3] Qianming Chen,[2,*] and J. Silvio Gutkind[1,*]

[1]Oral and Pharyngeal Cancer Branch, National Institute of Dental and Craniofacial Research, National Institutes of Health, Bethesda, MD 20892-4340, USA
[2]State Key Laboratory of Oral Diseases, West China Hospital of Stomatology, Sichuan University, Chengdu, Sichuan 610041, China
[3]Wilmer Eye Institute, Johns Hopkins School of Medicine, Baltimore, MD 21287, USA
[4]Fels Institute for Cancer Research and Molecular Biology, Temple University School of Medicine, Philadelphia, PA 19140, USA
[5]Schepens Eye Research Institute, Harvard Medical School, Boston, MA 02114, USA
[6]Laboratory of Cancer Biology and Genetics, National Cancer Institute, Bethesda, MD 20892, USA
*Correspondence: qmchen@scu.edu.cn (Q.C.), sg39v@nih.gov (J.S.G.)
http://dx.doi.org/10.1016/j.ccr.2014.04.016

SUMMARY

Mutually exclusive activating mutations in the *GNAQ* and *GNA11* oncogenes, encoding heterotrimeric Gαq family members, have been identified in ~83% and ~6% of uveal and skin melanomas, respectively. However, the molecular events underlying these *GNAQ*-driven malignancies are not yet defined, thus limiting the ability to develop cancer-targeted therapies. Here, we focused on the transcriptional coactivator YAP, a critical component of the Hippo signaling pathway that controls organ size. We found that Gαq stimulates YAP through a Trio-Rho/Rac signaling circuitry promoting actin polymerization, independently of phospholipase Cβ and the canonical Hippo pathway. Furthermore, we show that Gαq promotes the YAP-dependent growth of uveal melanoma cells, thereby identifying YAP as a suitable therapeutic target in uveal melanoma, a *GNAQ/GNA11*-initiated human malignancy.

INTRODUCTION

Mutations in *GNAQ* and *GNA11*, encoding two members of the Gαq family of heterotrimeric G protein α subunits, Gαq and Gα11, respectively, occur in roughly 5% of all tumors sequenced to date (O'Hayre et al., 2013). The majority of these mutations affect residues Q209 and R183, which are required for $G\alpha_q$ guanosine triphosphatase (GTPase) activity (Berman et al., 1996; Van Raamsdonk et al., 2010). Thus, the most frequent mutations observed in *GNAQ* and *GNA11* render them GTPase defective and constitutively active, leading to prolonged signaling. Of interest, ~83% of ocular melanomas harbor mutations in *GNAQ* or *GNA11*, where they are now considered to represent the driver oncogenes (Van Raamsdonk et al., 2009; Van Raamsdonk et al., 2010). This provides a clear example of a human malignancy that is initiated by gain-of-function mutations in $G\alpha_q$ and $G\alpha_{11}$ proteins. Although less studied, *GNAQ* and *GNA11* mutations are also frequently found in leptomeningeal melanocytomas (50%) and melanomas (25%) arising from the meninges (Küsters-Vandevelde et al., 2010), in most blue nevi of the skin (83%), and in a subset (6%) of cutaneous melanomas (Van Raamsdonk et al., 2009).

The best-known downstream signaling event initiated by Gαq involves its ability to activate phospholipase C (PLC) β and the

Significance

Uveal melanoma is the most frequent ocular malignancy in adults, for which no effective systemic therapies are currently available. Recent findings revealed that activating mutations in *GNAQ* and *GNA11*, encoding members of the Gαq family of G protein α subunits, drive uveal melanoma oncogenesis. Here we report that *GNAQ* stimulates the transcriptional coactivator YAP in human uveal melanoma cells and *GNAQ*-induced cancer mouse models. At the molecular level, Gαq activates YAP by acting on a Hippo-independent signaling network initiated by actin polymerization. Ultimately, YAP is essential for uveal melanoma cell proliferation, thereby rendering it sensitive to clinically relevant small-molecule YAP inhibitors. Hence, this cancer vulnerability can be exploited for the development of new precision molecular therapies for *GNAQ*-driven human malignancies.

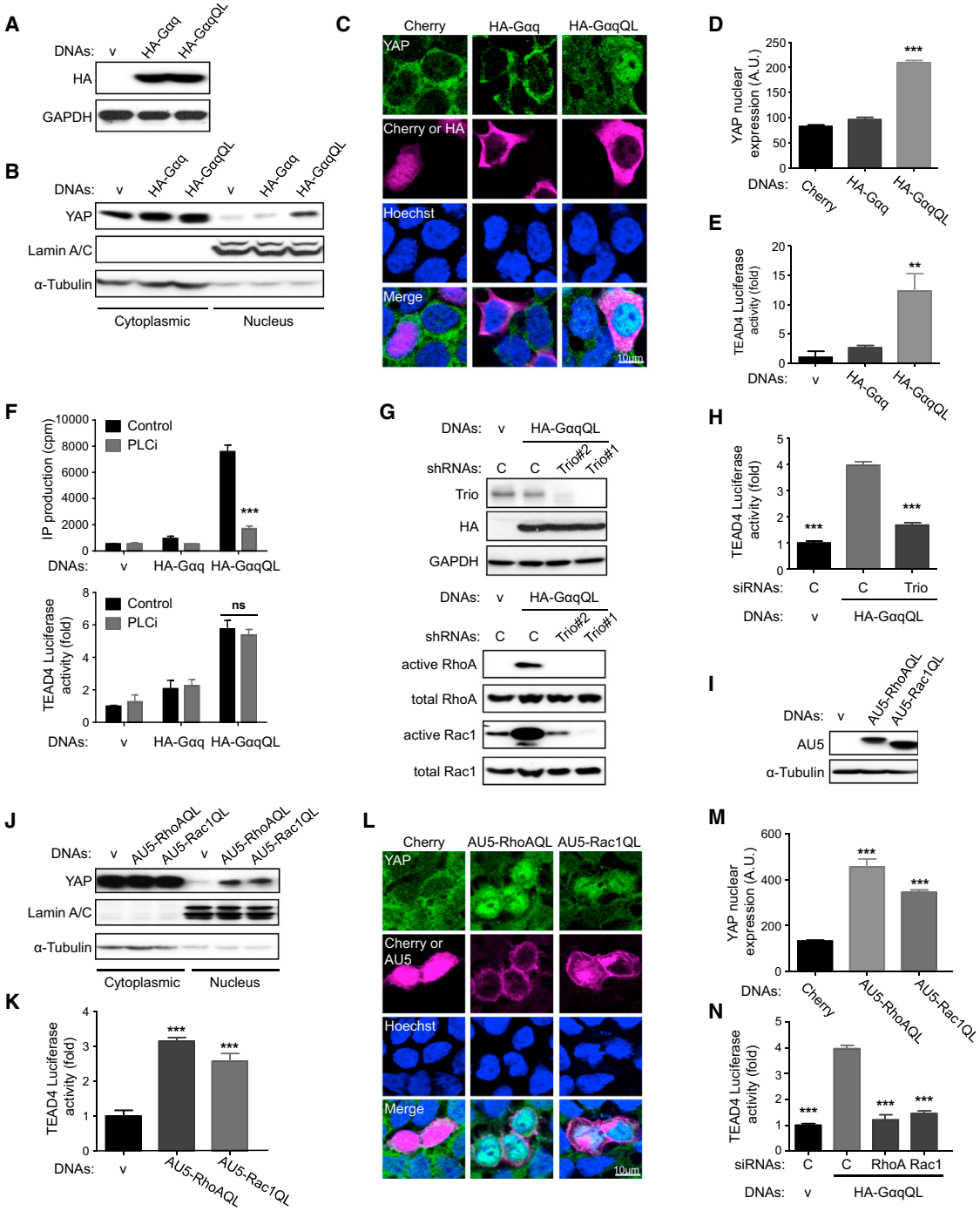

Figure 1. Activating Mutations in Gαq—GαqQL—Induce YAP Nuclear Translocation and YAP-Dependent Transcription Activation through Trio and Trio-Dependent Rho-GTPases

(A) Western blots show HA-Gαq and HA-GαqQL expression in HEK293 cells transfected with HA-Gαq or HA-GαqQL expression vectors (DNAs), using endogenous glyceraldehyde 3-phosphate dehydrogenase as a loading control.

(B) Western blot shows YAP expression levels in the nuclear fraction; enrichment for lamin A/C and α tubulin served as nuclear and cytoplasmic markers respectively.

(C and D) Immunofluorescence shows that transfected GαqQL induces YAP nuclear translocation, but not Gαq or mCherry. (C) Endogenous YAP (green) was detected by immunofluorescence along with Hoechst for nuclear DNA (blue) and HA staining (violet) or mCherry (violet, as control). (D) Nuclear YAP in HA-positive and mCherry-positive cells was quantified with ImageJ and represented as arbitrary units in the indicated cell populations (mean ± SEM, n = 50–100 cells).

(E) HEK293 cells were cotransfected with HA-Gαq or HA-GαqQL and Gal4-TEAD4, 5 × UAS-Luc and Renilla-Luc DNAs followed by luciferase assay (mean ± SEM, n = 3).

(legend continued on next page)

consequent increased hydrolysis of phosphatidylinositol 4,5-bisphosphate to produce two second messengers: inositol 1,4,5-trisphosphate (IP_3) and diacylglycerol (DAG) (Hubbard and Hepler, 2006). IP_3 raises cytoplasmic Ca^{2+} levels, which stimulates multiple calcium-regulated pathways and, together with DAG, activates classic protein kinase C isoforms (Griner and Kazanietz, 2007). However, the molecular events underlying *GNAQ*-driven malignancies are not yet defined, thus limiting the ability to develop novel anticancer-targeted therapies. Here, we focused on the transcriptional coactivator YAP, a critical component of the Hippo signaling pathway that controls organ size in mammals (Pan, 2010; Ramos and Camargo, 2012; Sudol et al., 1995; Zhao et al., 2010). YAP is active in most proliferating cells, but upon reaching the appropriate cell density, signaling pathways initiated upon cell-cell contact and/or from the organ size-sensing machinery lead to the activation of the Hippo kinase cascade, resulting in the inhibitory activity of the mammalian STE20-like protein kinases 1 and 2, which are the mammalian homologs of Hippo in *Drosophila melanogaster* (Pan, 2010; Ramos and Camargo, 2012; Zhao et al., 2010). This pathway converges in the activation of a kinase known as large tumor suppressor homolog 1 and 2 (LATS1 and LATS2 in humans), which phosphorylates YAP in serine 127, thereby targeting it for retention and degradation in the cytosol and thus limiting its transcriptional activity and resulting in growth inhibition (Camargo et al., 2007; Dong et al., 2007; Pan, 2010; Ramos and Camargo, 2012).

In this study, we show that activating mutation of Gαq can trigger YAP translocation into the nucleus and stimulate YAP-dependent transcription and that this process is independent from PLCβ stimulation but requires the activation of a Gαq-regulated guanine nucleotide exchange factor, Trio, and the subsequent activation of the small GTPases RhoA and Rac1 and their associated signaling networks. In turn, this Gαq-Trio-Rho/Rac signaling circuitry contributes to the YAP-dependent growth in uveal melanoma, thus identifying suitable therapeutic targets for uveal melanoma treatment.

RESULTS

YAP Activation Downstream of Oncogenic Activating Mutants of Gαq—GαqQL—through RhoA and Rac1

To assess the expression and localization of the transcriptional coactivator YAP in response to activating mutations in *GNAQ*, we transfected human embryonic kidney 293 (HEK293) cells with human influenza hemagglutinin A epitope (HA)-tagged GαqQL (Q209L), one of the most frequent *GNAQ* mutants in uveal melanoma (O'Hayre et al., 2013), using empty vector and wild-type Gαq as controls. Both tagged G protein α subunits were expressed at similar levels (Figure 1A), but only the active Gαq protein promoted the nuclear translocation of YAP, as judged by its increased recovery in the nuclear fraction (Figure 1B) and by YAP immune detection in the nuclei of transfected cells, which could be recognized by staining of the HA tag in the background of untransfected cells (Figures 1C and 1D). GαqQL also caused a remarkable increase in the luciferase activity of a YAP reporter system driven by a TEAD4-Gal4 chimera, which included the TEAD4 transactivation and YAP-binding domain, and promoted the expression of endogenous YAP-regulated genes, including *CTGF* and *CYR61* (Figure 1E; Figure S1A available online). These results, together with recently reported biochemical studies (Yu et al., 2012), support that *GNAQ*-activating signaling can lead to YAP nuclear translocation and YAP-dependent activating gene transcription.

However, it is unclear which of the multiple Gαq-initiated pathways regulate YAP and how the interplay between YAP and other *GNAQ*-initiated signaling pathways contributes to the transduction of proliferative cues by this G protein and its coupled receptors. The activation of PLCβ is one of the best-known downstream events stimulated by Gαq. Inhibition of PLCβ by the use of a small-molecule PLC inhibitor (PLCi) abolished the generation of diffusible second messengers but did not affect the transcriptional activation of YAP by Gαq (Figure 1F; Figure S1B), demonstrating that activation of YAP may be independent of PLCβ.

In a recent study, a genome-wide double-stranded RNA screen in *Drosophila* cells revealed that Trio, a highly conserved guanine nucleotide exchange factor, is essential for transducing signals from Gαq to the AP1 transcription factors through the activation of Rho-GTPases and their signaling circuitries (Vaqué et al., 2013). These findings prompted us to investigate whether Trio and its regulated Rho GTPases, RhoA and Rac1, participate in the nuclear translocation and activation of YAP in response to Gαq-activating mutations. Knockdown of Trio did not affect the expression levels of GαqQL but abolished its ability to promote the accumulation of activated RhoA and Rac1 (Figure 1G). Knockdown of Trio also prevented the activation of the YAP transcriptional activity caused by GαqQL (Figure 1H; Figure S1C).

(F) HEK293 cells were transfected with HA-Gαq or HA-GαqQL, followed by PI turnover assays (mean ± SEM, n = 6) (upper panel) or cotransfected with Gal4-TEAD4, 5 × UAS-Luc and Renilla-Luc DNAs, followed by PLCi treatment (1 hr) and luciferase assay (mean ± SEM, n = 3) (lower panel).
(G) Transfected HA-GαqQL or vector into shRNA-control, shRNA-Trio#1, and shRNA–Trio#2 HEK293 cells, followed by the indicated western blot analysis (upper panel) or by RhoA and Rac1 small GTPase activation assays (lower panels).
(H) HEK293 cells were cotransfected with siRNA Trio or control and HA-GαqQL or vector and Gal4-TEAD4, 5 × UAS-Luc, and Renilla-Luc DNAs, followed by luciferase assay (mean ± SEM, n = 6).
(I) Western blot shows AU5-RhoAQL and AU5-Rac1QL expression in HEK293 cells transfected with the corresponding expression plasmids.
(J) Western blots show that both RhoAQL and Rac1QL can induce YAP accumulation in the nuclear fraction, using enrichment in lamin A/C and α tubulin as nuclear and cytoplasmic markers, respectively.
(K) HEK293 cells were cotransfected with AU5-RhoAQL or AU5-Rac1QL and Gal4-TEAD4, 5 × UAS-Luc, and Renilla-Luc DNAs, followed by luciferase assays (mean ± SEM, n = 6).
(L and M) Immunofluorescence assay and nuclear YAP quantification, using the procedure described in (C) in the indicated transfected cells (mean ± SEM, n = 50–100 cells).
(N) HEK293 cells were cotransfected with siRNAs RhoA, Rac1, or control and HA-GαqQL or vector and Gal4-TEAD4, 5 × UAS-Luc, and Renilla-Luc DNAs, followed by luciferase assay, as above (mean ± SEM, n = 6).
See also Figure S1.

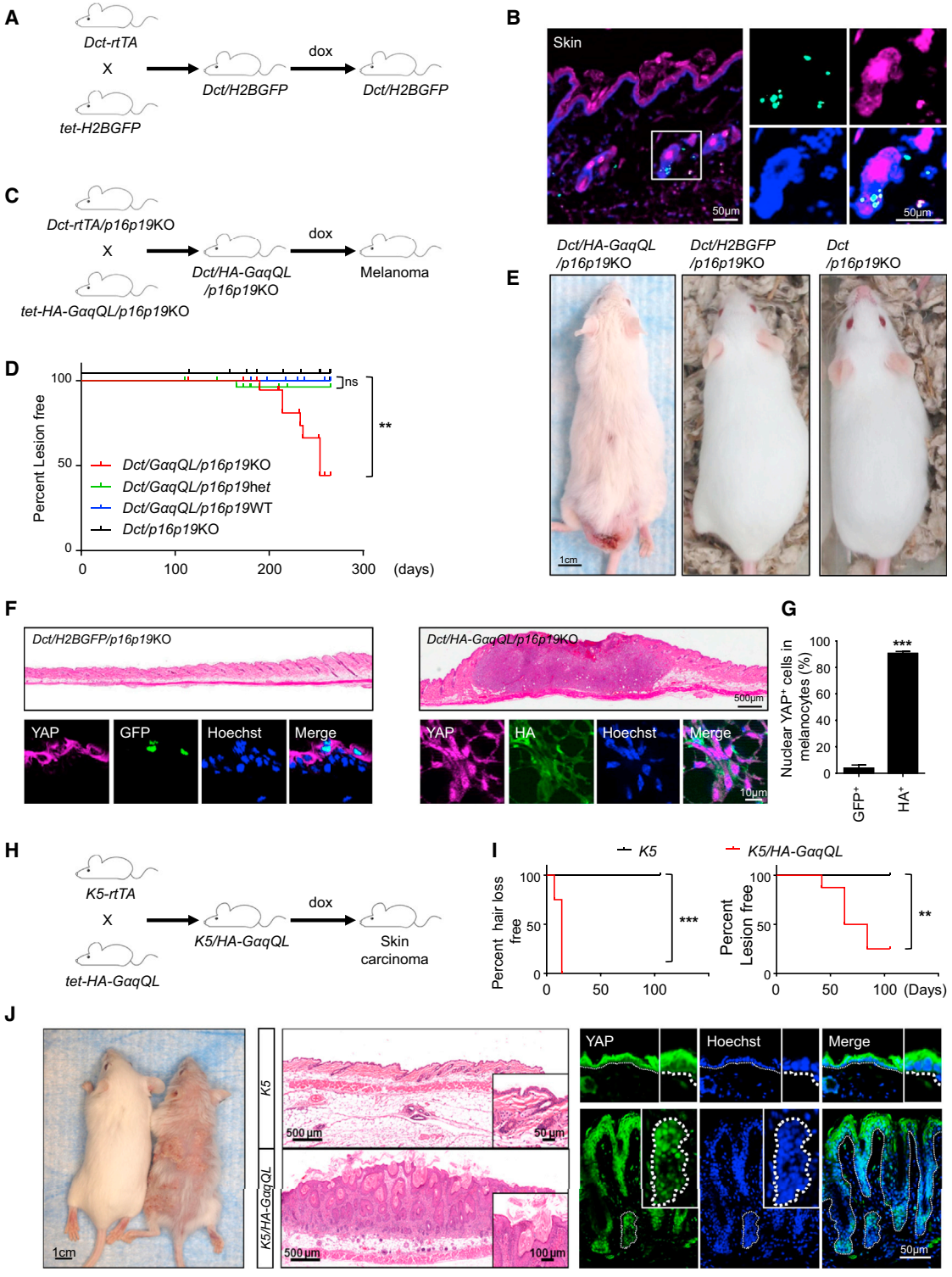

Figure 2. Conditional Expression of the GαqQL Promotes Melanoma or Skin Carcinoma Formation and YAP Activation In Vivo

(A) *Dct-rtTA* mice were bred with *tet-H2BGFP* transgenic mice to produce inducible *Dct/H2BGFP* double-transgenic mice, which express GFP exclusively in melanocytes, when fed with doxycycline food (dox).

(B) *Dct/H2BGFP* mice show tight regulation GFP expression in skin melanocytes (green), using Hoeschst and phalloidin to stain nuclear DNA (blue) and cytoplasmic polymerized actin (red), respectively (as shown in Zaidi et al., 2011).

(C) *Dct-rtTA/p16p19*KO mice were bred with *tet-HA-GαqQL/p16p19*KO mice to produce inducible *Dct/HA-GαqQL/p16p19*KO mice, which expressed HA-GαqQL exclusively in melanocytes, when fed with doxycycline food.

(legend continued on next page)

However, although the activation of YAP by activated RhoA has been recently reported (Yu et al., 2012), we observed that Rac1 can also stimulate the nuclear translocation of endogenous YAP and its transactivating activity when expressed together with the GAL4-TEAD4 reporter system (Figures 1I–1M). Interestingly, knockdown of either of these two Rho-GTPases prevented the transcriptional activation of YAP induced by GαqQL (Figure 1N; Figures S1D and S1E). Thus, although the activated mutants of either RhoA or Rac1 can activate YAP, the concomitant activation of both endogenous GTPases appears to be required for the full stimulation of endogenous YAP when activated by oncogenic forms of Gαq.

Conditional Expression of the *GNAQ* Oncogene Promotes Melanoma Formation and YAP Activation In Vivo

To investigate whether activated *GNAQ* can drive melanocyte transformation in vivo, we generated a mouse model expressing HA-GαqQL under the control of the *tet*-responsive elements (tet-HA-GαqQL) and bred them with mice expressing the reverse tetracycline-activated transactivator rtTA2, regulated by the melanocyte-specific dopachrome tautomerase (*Dct*) gene promoter (*Dct-rtTA*) (Zaidi et al., 2011). Initially, we used the nuclear expression of a *tet*-driven H2B-GFP to document the targeted expression to skin melanocytes by *Dct-rtTA* (Figures 2A and 2B), as previously reported (Zaidi et al., 2011). The *tet-HA-GαqQL* and *Dct-rtTA* transgenic mice were also bred with mice defective in $p16^{Ink4a}$ and $p19^{Ink4b}$ (*p16p19*KO) (Figure 2C), as genetic and epigenetic inactivation of this tumor suppressive pathway is a frequent event in uveal and cutaneous melanoma (Castellano et al., 1997; van der Velden et al., 2001). This was reflected by the methylation of the *Ink4 (CDKN2)* gene promoter region in a representative panel of human melanoma cells lines (Figure S2). Using this animal model system, we observed that when HA-GαqQL was expressed in response to doxycycline treatment in the *p16p19*KO background, more than 50% of the mice developed cutaneous lesions of melanocytic origin expressing Dct (Figures 2D and 2E and data not shown). This is aligned with the finding that hot-spot mutations in *GNAQ* and its related *GNA11* are mutated in 5% of all cutaneous melanomas (O'Hayre et al., 2013; Van Raamsdonk et al., 2009), which on the basis of our observations may represent a tumor-initiating genetic event. In these lesions, most HA-GαqQL expressing cells exhibit nuclear YAP, in contrast to normal tissues, in which control GFP expressing melanocytes exhibit cytoplasmic YAP (Figures 2F and 2G). Thus, mutated *GNAQ* can initiate melanocyte transformation and tumor formation in mice when expressed in a progenitor cell compartment and results in YAP nuclear localization in vivo. As *GNAQ* mutations have been identified in other tumors, we expressed HA-GαqQL in the skin, including the hair follicle stem cells, using a cytokeratin 5 (*K5*) *rtTA* diver (Figure 2H) (Vitale-Cross et al., 2004). These mice developed rapid hair loss within days and exhibited nuclear localization of YAP in epithelial-derived hyperplastic cells in multiple tumor lesions (Figures 2I and 2J). Collectively, these results suggest that YAP activation in tumors initiated by activating mutations of Gαq is likely a general event, not restricted to melanocyte progenitor cells and their derived tumors.

Trio and a Network of Rho-GTPases Mediate YAP Activation in Uveal Melanoma Cells Harboring *GNAQ* Mutations

We next examined the expression of YAP in human uveal melanoma lesions. Consistent with our experimental findings, we observed that YAP accumulates in the nucleus in human uveal melanoma lesions (Figures 3A and 3B). In contrast, normal melanocytes do not express nuclear YAP in normal tissues. This suggests that YAP may contribute to the oncogenic pathway initiated by *GNAQ*- and *GNA11*-activating mutations in human uveal melanomas. On the basis of these observations, we next asked whether YAP is activated in uveal melanoma cells expressing the *GNAQ* oncogene. Indeed, uveal melanoma cells exhibited clear nuclear-localized YAP, which was insensitive to PLC inhibition, similar to HEK293-expressing active Gαq, even when PLCi was used to effectively block phosphatidylinositol hydrolysis (Figures 3C and 3D). The nuclear localization of YAP was abolished after *GNAQ* knockdown in uveal melanoma cell lines (Figures 3E and 3F). Similarly, knockdown of Trio, RhoA, and Rac1 prevented the nuclear accumulation of YAP in these cells and diminished the expression of endogenous YAP-regulated genes, *CTGF* and *CYR61* (Figures 3E–3G). These findings support that in uveal melanoma cells harboring *GNAQ* mutations, Gαq primarily signals through Trio to RhoA and Rac1 to promote the nuclear localization and activation of YAP, independent of PLC activation and its downstream regulated events.

Surprisingly, uveal melanoma cells displayed very high levels of total and phosphorylated (serine 127) YAP. The latter likely represents the YAP-inactive form upon phosphorylation by LATS1 and LATS2, which are highly expressed in these cells, similar to cutaneous melanoma cells expressing *BRAF* and *NRAS* oncogenes, which served as controls. LATS1 was also recognized by antibodies detecting its phosphorylated form at the hydrophobic motif (T1079) and activation loop (S909) both in uveal melanoma cells and in HEK293 cells expressing

(D) Percentage of mice developing cutaneous lesions of melanocytic origin after feeding with doxycycline food.
(E) Example of Dct/HA-GαqQL/p16p19KO mice developing lesions in the skin.
(F) Histology shows *Dct/HA-GαqQL/p16p19*KO mouse with cutaneous melanoma (upper right panel). Immunofluorescence assay of frozen tissues shows that HA-GαqQL (green) positive cells display YAP (violet) nuclear translocation using Hoechst for DNA staining (blue) (right lower panel). Normal skin from *Dct/H2BGFP* mouse stained with GFP (green) instead of HA as control (left lower panel) shows cytoplasmic YAP.
(G) Quantification of percentage nuclear YAP-positive cells in GFP- or HA-positive cells (GFP^+ and HA^+, respectively).
(H) *K5-rtTA* mice were bred with *tet-O-HA-GαqQL* mice to produce inducible *K5/HA-GαqQL* mice, which express HA-GαqQL exclusively in basal epithelial cells (Vitale-Cross et al., 2004), when fed with doxycycline food.
(I) *K5/HA-GαqQL* mice developed rapid hair loss within days (left) and exhibited multiple tumor lesions on the skin (right).
(J) Histology showed that these *K5/HA-GαqQL* mice developed skin carcinoma (middle lower panel). Immunofluorescence assays in frozen tissues show that *K5/HA-GαqQL* mice exhibit YAP (green) nuclear translocation, using Hoechst to stain nuclear DNA (blue) (right lower panels).
See also Figure S2.

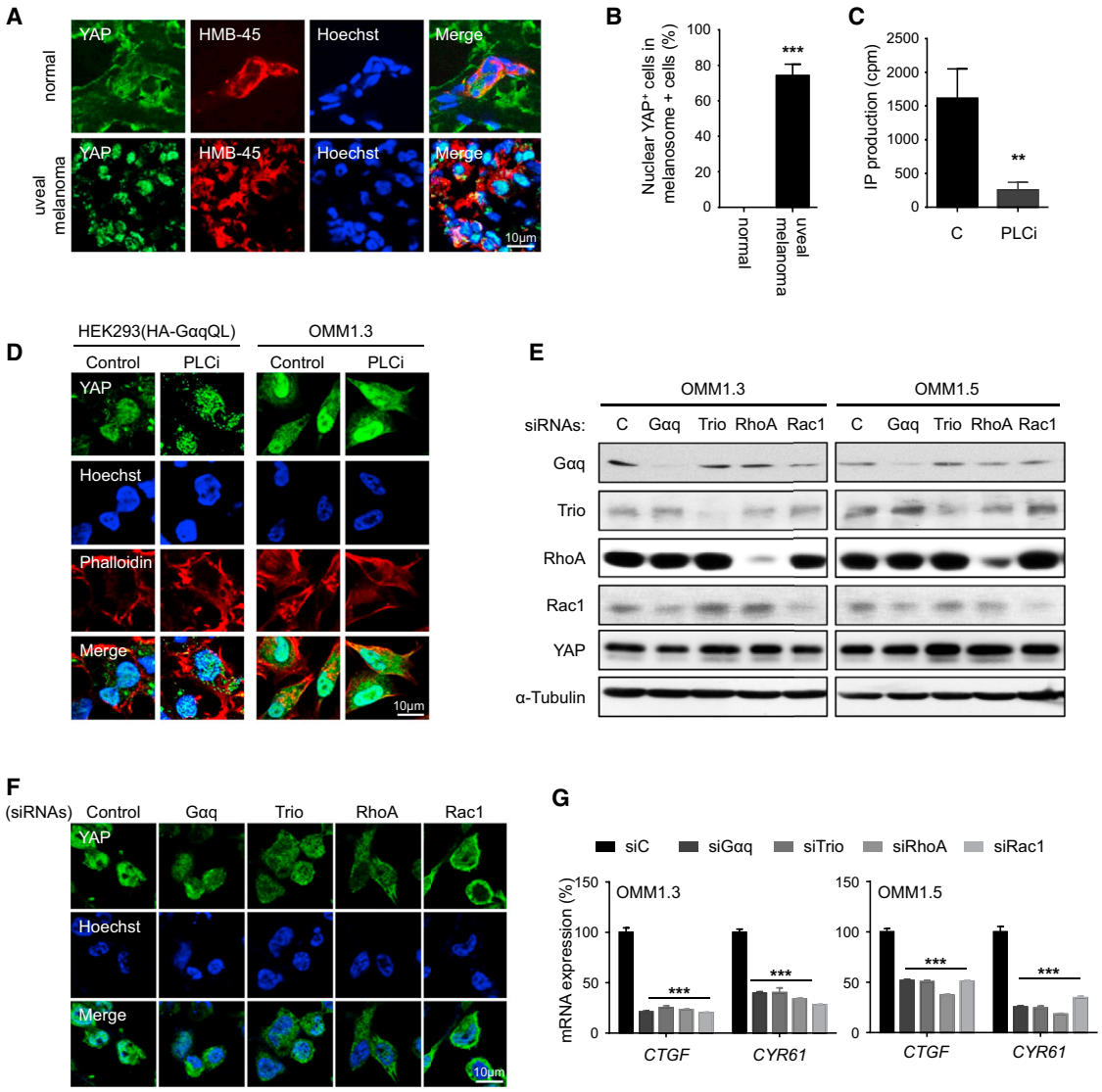

Figure 3. Trio and a Network of Rho-GTPases Mediate YAP Activation in Uveal Melanoma Cells Harboring *GNAQ* Mutations

(A) Immunofluorescence assays using frozen tissues from clinical uveal melanoma specimens (n = 6) showed HMB-45-positive cells (red) with nuclear YAP (green), using Hoechst to stain nuclear DNA (blue), using as control HMB-45 staining to identify the resident melanocytes in normal tissues (n = 3).

(B) Quantification of percentage nuclear YAP-positive cells in melanosome-positive cells.

(C) PLCi inhibits the hydrolysis of PIs in OMIM1.3 uveal melanoma cells as judged by PI turnover assays.

(D) HEK293 cells transfected with GαqQL expression vectors and OMM1.3 uveal melanoma cells exhibited nuclear YAP by immunofluorescence (green), which was insensitive to PLC inhibition, using Hoechst and phalloidin to stain nuclear DNA (blue) and cytoplasmic polymerized actin (red), respectively.

(E) Western blot analysis documents knockdown using siRNAs in two uveal melanoma cell lines.

(F) OMM1.3 uveal melanoma transfected with siRNA control show cells with YAP (green) nuclear staining, while cells transfected with the indicated siRNAs show YAP mainly localized to the cytoplasm. Hoechst stains nuclear DNA (blue).

(G) siRNA knockdown of Gαq, Trio, RhoA, or Rac1 diminishes the expression of endogenous YAP-regulated genes (*CTGF* and *CYR61*) in OMM1.3 and OMM1.5 uveal melanoma cells (mean ± SEM, n = 3).

GNAQ (Figure 4A). *GNAQ* expression in HEK293 cells resulted in the accumulation of dephosphorylated YAP, reflected by the faster migration of YAP in Phos-tag-containing gels, with only dephosphorylated YAP accumulating in the nucleus (Figure 4B). All uveal melanoma cells also accumulated dephosphorylated YAP, although they still retained phospho-YAP (Figures 4A and 4C). Together, these observations suggested that LATS1/LATS2 may remain active in uveal melanoma cells and raised the possibility that YAP activation by *GNAQ* may involve mechanisms in addition to those described resulting in Hippo pathway inactivation and LATS1/2 inhibition (Yu et al., 2012).

To explore this possibility, we knocked down LATS1/2 in HEK293 cells, which alone induced only a slight increase in YAP transcriptional activity in confluent cells. Interestingly, the *GNAQ* oncogene induced the transcriptional activation of YAP even when the repressing signals converging on LATS1/2

were suppressed by knockdown of both human LATS isoforms (Figures 4D–4F), supporting that activation of YAP by GαqQL is not solely dependent on the inhibition of the Hippo pathway. Recently, a likely Hippo-independent pathway resulting in the activation of YAP initiated by actin polymerization was described in the context of cell mechanical sensing (Aragona et al., 2013; Dupont et al., 2011; Halder et al., 2012). Aligned with the strong activation of RhoA and Rac by GαqQL, uveal melanoma cells exhibit high levels of phosphorylated cofilin (p-cofilin) (Figure 4G), a downstream target of both of these GTPases (Figures 4H and 4I). Accumulation of p-cofilin results in increased actin polymerization and the consequent increase in polymerized F-actin and decrease in monomeric G-actin (Bernard, 2007; Pollard and Cooper, 2009). Remarkably, YAP nuclear localization and activity were repressed when blocking actin polymerization by inhibiting ROCK, thereby limiting cofilin phosphorylation specifically downstream of RhoA or by the direct inhibition of G-actin assembly into F-actin by latrunculin-A (Lat.A) (Figures 4J–4M; Figure S3). Together, these findings suggest that *GNAQ* may stimulate YAP by promoting actin polymerization rather than by solely inhibiting the canonical Hippo pathway.

A Hippo-Independent Pathway Regulated by Actin Polymerization Contributes to YAP Activation in Uveal Melanoma

We next explored the interplay between the Hippo pathway and actin polymerization in YAP activation. Knockdown of LATS1/2 resulted in a remarkable increase in the expression of YAP-regulated genes in uveal melanoma cells, further supporting that the Hippo pathway remains active in these cells, restraining maximal YAP activation (Figures 5A and 5B). Even when LATS1/2 was knocked down, inhibition of actin polymerization decreased YAP activity, both in uveal melanoma and GαqQL transfected cells (Figures 5B–5D), suggesting that F-actin accumulation and LATS inhibition may act in a coordinated fashion. Regarding the former, how actin polymerization results in YAP stimulation is complex and not fully understood (Aragona et al., 2013; Dupont et al., 2011; Halder et al., 2012; Johnson and Halder, 2014). Recent studies suggest that YAP may form many multimeric protein complexes using its WW domains, a leucine zipper and PDZ-binding motif (Sudol, 2013; Sudol et al., 2012; Wang et al., 2014). Of interest, these include the association of YAP with a cytoskeletal-associated protein, angiomotin (AMOT), which binds F-actin through an N-terminal region that includes a sequence motif, PPxY, by which AMOT associates with WW domains of YAP (Oka et al., 2012; Chan et al., 2013; Dai et al., 2013). We reasoned that F-actin may prevent AMOT's associating with YAP and that upon inhibition of actin polymerization, YAP may be sequestered in an inactive, AMOT-associated pool. Preventing actin polymerization in uveal melanoma cells did not enhance protein complex formation between flag-tagged YAP and endogenous LATS or 14-3-3, both of which repress YAP function (Figure 5E). Instead, YAP association with the endogenous p130 form of AMOT was increased after inhibition of actin polymerization (Figure 5E). This could be recapitulated in vitro, as AMOT bound to flag-YAP was competed out by incubating the immunoprecipitates with F-actin but not G-actin (Figure 5F). Consistently, AMOT knockdown had limited impact on YAP-dependent gene expression in uveal melanoma cells, as it is expected to bind YAP poorly in the presence of cytosolic F-actin, but AMOT knockdown rescued YAP function inhibition caused by actin depolymerization (Figures 5G and 5H). Taken together, these findings suggest that in uveal melanoma cells, F-actin accumulation causes the dissociation of AMOT-YAP complexes, thereby contributing to YAP nuclear translocation and YAP-dependent transcription (Figure 5I).

YAP Represents a Therapeutic Target in Uveal Melanoma

We next explored the role of YAP activation in uveal melanoma tumor formation. For these studies, we established lentiviral-delivered small hairpin RNAs (shRNAs) knocking down YAP and control shRNA in uveal melanoma cells. This approach revealed that YAP knockdown resulted in reduced YAP-dependent expression of typical YAP-regulated genes (Mo et al., 2012) and decreased the proliferation of uveal melanoma cells (Figures 6A–6C). Furthermore, knockdown of YAP led to a reduced number of colonies in uveal melanoma cells cultured in 3D matrix, as well as a reduced colony size (Figure 6D). Taking advantage of the ability to establish uveal melanoma xenografts in immune compromised mice, we observed that YAP knockdown reduced tumor size in vivo (Figure 6E). Taken together, these results suggest that YAP activation may represent a molecular event involved in uveal melanoma tumor growth in vitro and in vivo.

These observations raised the possibility that YAP may represent a therapeutic target for the treatment of patients with uveal melanoma. On the basis of the identification of verteporfin (VP) as a potent inhibitor of the YAP-TEAD4 interaction in a recent high-throughput drug screen (Liu-Chittenden et al., 2012), we asked whether VP can exert an antitumoral activity in uveal melanoma cell lines. VP treatment reduced colony formation and proliferation of uveal melanoma cells in soft agar 3D cultures (Figure 6F) and dramatically reduced uveal melanoma cell tumorigenesis and proliferation in vivo (Figures 6G and 6H). These results suggest that the pharmacological inhibition of YAP by VP may represent as a therapeutic approach for the treatment of patients with uveal melanomas.

DISCUSSION

Recent large cancer-sequencing efforts have revealed an unexpected high frequency of gain-of-function mutations in heterotrimeric G protein α subunits (O'Hayre et al., 2013). Among them, mutations in the *GNAQ* oncogenes, *GNAQ* and *GNA11*, are now believed to represent the genetic initiating event in uveal melanomas and in a subset of melanomas arising in the skin (Van Raamsdonk et al., 2009; Van Raamsdonk et al., 2010), among other tumors. In this study, we show that YAP activation represents a key molecular event contributing to *GNAQ*-induced tumorigenesis, which is dependent on the activation of Trio and its regulated Rho GTPases, RhoA and Rac1, in uveal melanoma cells harboring activating *GNAQ* mutations. Furthermore, we provide evidence that YAP activation may involve, at least in part, a Hippo-independent pathway impinging on the regulation of the actin cytoskeleton by Rho GTPases. These findings suggest that inhibition of YAP function may represent a suitable pharmacological intervention strategy in uveal melanoma and other hyperproliferative lesions that result from gain-of-function *GNAQ* mutations.

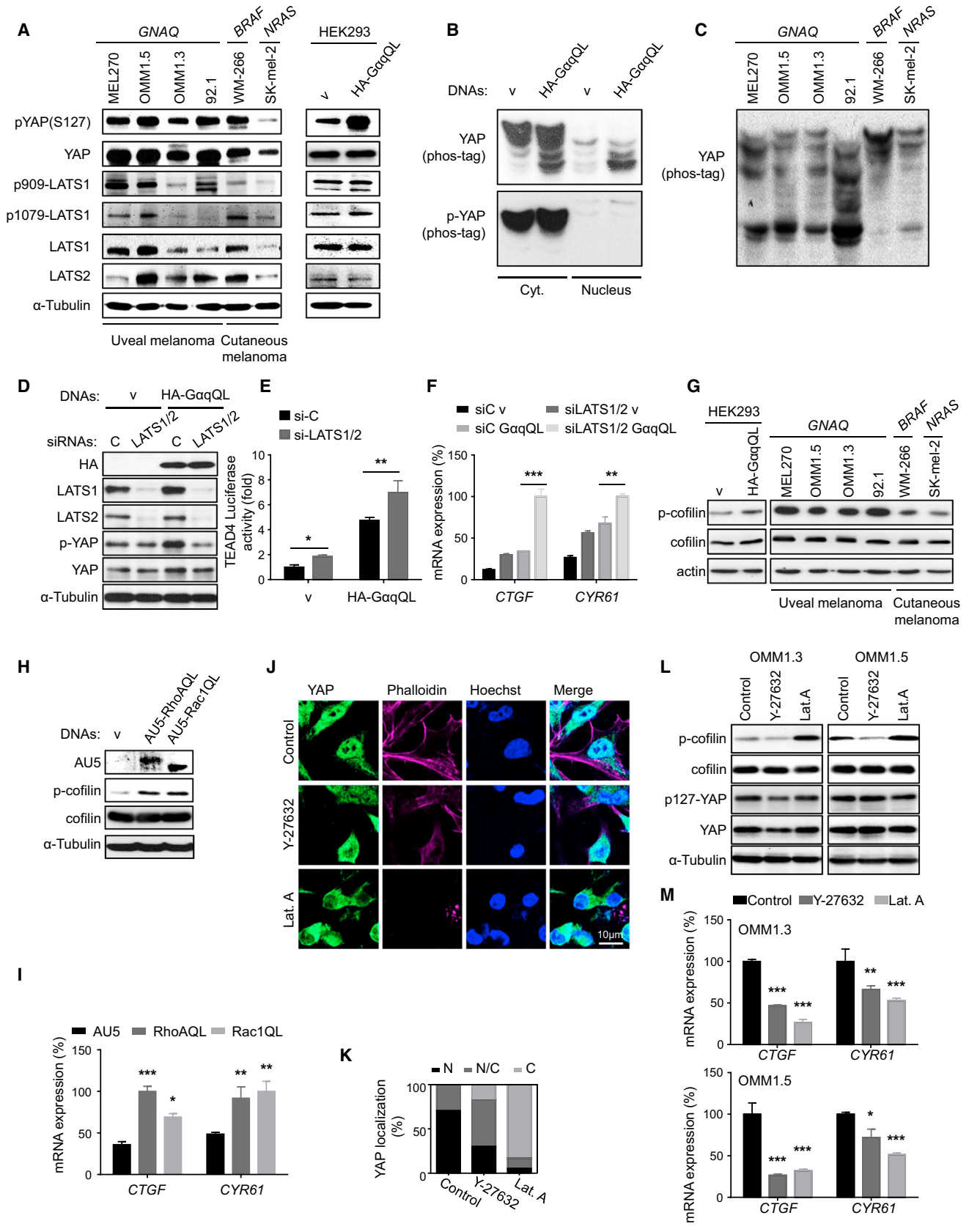

(legend on next page)

YAP is a transcriptional coactivator that acts as a powerful tumor promoter, and its activation is a frequent event in numerous cancers, including lung, colorectal, ovarian, liver, and prostate cancers (Dong et al., 2007; Johnson and Halder, 2014; Zhao et al., 2007). The Hippo pathway is believed to be the major regulator of YAP nuclear localization, activity, and tumorigenic potential (Camargo et al., 2007; Dong et al., 2007; Pan, 2010; Ramos and Camargo, 2012; Zhao et al., 2010). YAP and its *D. melanogaster* counterpart Yorkie (YKI) promote tissue growth and cell viability by regulating the activity of different transcription factors, including TEADs and SMADs. In mammals, YAP overexpression or hyperactivation causes excess proliferation in multiple tissues, including the liver, gastrointestinal tract, skin, and heart (Camargo et al., 2007; Dong et al., 2007; Schlegelmilch et al., 2011). Despite this, somatic or germline mutations in Hippo pathway genes are uncommon, prompting the exploration of other mechanism(s) underlying YAP activation in each tumor type (Johnson and Halder, 2014).

Recent studies suggest that G protein-coupled receptor (GPCR) signaling can regulate the Hippo pathway (Yu et al., 2012). Specifically, GPCRs linked to $G\alpha_{12/13}$ inhibit the activity of LATS, thereby relieving YAP from the LATS-dependent inhibitory phosphorylation in serine 127 (Yu et al., 2012), while receptors activating Gαs may promote LATS activation, thus causing YAP inhibition by increasing Hippo pathway activation. Whether *GNAQ*-activating mutations and the large family of receptors regulating cell growth through Gαq affect the Hippo pathway, however, is much less understood (Yu et al., 2012). In our study, we found that YAP is a key protumorigenic gene in uveal melanoma cells harboring *GNAQ* activating mutations, which is critical for uveal melanoma growth and tumor formation as judged by knockdown experiments and by the use of small-molecule inhibitors. Moreover, we also showed that activation of YAP downstream of Gαq occurs through the stimulation of Trio and Trio-dependent-Rho GTPases, RhoA and Rac1. Of interest, Gαq activation did not result in decreased levels of phosphorylated LATS and YAP, and Gαq activated YAP further even when LATS was knocked down in both uveal melanoma and HEK293 cells. Instead, our results suggest that Gαq stimulates YAP by a process involving changes in actin dynamics rather than solely by Hippo kinase cascade regulation, resembling recent findings in the context of mechanosensing transduction signals (Aragona et al., 2013; Dupont et al., 2011; Halder et al., 2012).

In this regard, whereas in *Drosophila*, most of the key components of the Hippo pathway have been genetically defined, in mammalian cells, YAP may receive negative and positive inputs from multiple signaling systems in addition to those described in flies. For example, a recent kinome-wide screen in mammalian cells revealed that the tumor suppressor protein LKB1 inhibits YAP by activating the core Hippo kinases, while members of the c-Jun N-terminal kinase pathway diminish YAP function independently of Hippo (Mohseni et al., 2014). The regulation of YAP by the cytoskeleton in *Drosophila* involves the tumor suppressor Merlin/NF2, which can cause the activation of *Drosophila* LATS (*Wts*) and hence activate the Hippo pathway, diminishing Yki activity upon the disruption of the cytoskeleton (Yin et al., 2013). Although this repressive function is also likely performed by NF2 in mammals, the activation of YAP by mechanosensing mechanisms appears not to require LATS inhibition, as supported by multiple experimental approaches (Aragona et al., 2013; Dupont et al., 2011). Similarly, active Gαq, RhoA, and Rac1 stimulated YAP potently even when endogenous LATS1/2 were efficiently knocked down. In line with this possibility, in uveal melanoma cells, LATS1 is phosphorylated in its activation loop, while LATS1/2 knockdown results in a remarkable increase in the transcriptional activity of YAP, indicating that these core Hippo kinases retain a restraining activity on YAP function. Instead, disruption of the actin cytoskeleton diminishes both the basal activity of YAP and YAP hyperactivation caused by LATS1/2 reduced expression. Thus, YAP stimulation by *GNAQ* in uveal melanoma cells requires the persistent activation of a cytoskeleton-regulated pathway, which may cooperate with or bypass the requirement of Hippo pathway inactivation.

The fact that RhoA and Rac1 stimulate YAP, albeit RhoA more potently, may provide some possible hints on the underlying mechanism. Although these GTPases often act antagonistically

Figure 4. *GNAQ* Oncogenic Signaling Induces YAP Nuclear Translocation and YAP-Dependent Transcription Activation through Rho-GTPases and Actin Remodeling

(A) Western blots show expression of total and phosphorylated (serine 127) YAP and LATS1 and LATS2 in uveal and cutaneous melanoma cells, the latter expressing *BRAF* and *NRAS* oncogenes, as indicated, as well as in HEK293 cells expressing GαqQL or vector (v) as controls.

(B and C) Cell lysates were subjected to immunoblotting with the indicated antibodies. Gels containing phos-tag were used to assess YAP phosphorylation status. Dephosphorylated YAP was reflected by the faster migration of YAP. (B) Phosphorylated YAP (p-YAP and slower mobility forms) and dephosphorylated YAP in the cytosolic (Cyt.) and nuclear (Nucleus) fractions of HEK293 cells transfected with GαqQL or vector control. (C) Phosphorylated YAP (slower mobility forms) in uveal and cutaneous melanoma cells expressing the indicated oncogenes.

(D) HEK293 cells were cotransfected with siRNA LATS1 and LATS2 or control and HA-GαqQL or vector DNAs, followed by the indicated western blot analysis for HA-Gαq, LATS1, LATS2, p(127)-YAP, YAP, and α tubulin as a loading control.

(E) Similarly, cells were also transfected with Gal4-TEAD4, 5 × UAS-Luc, and Renilla-Luc DNAs, followed by luciferase assay (mean ± SEM, n = 3).

(F) Cells were also studied by qPCR to assess the expression levels of YAP-regulated genes (*CTGF* and *CYR61*) (mean ± SEM, n = 3).

(G) Levels of cofilin and p-cofilin in HEK293 cells expressing GαqQL or vector control, as well as in the indicated uveal and cutaneous melanoma cells.

(H) Accumulation of phosphorylated cofilin in HEK293 cells expressing RhoAQL or Rac1QL.

(I) Expression of YAP-regulated genes (*CTGF* and *CYR61*) in HEK293 cells expressing RhoAQL or Rac1QL (mean ± SEM, n = 3).

(J) OMM1.3 uveal melanoma cells treated with Y-27632 or Lat.A, following with immunofluorescence assay, YAP (green), Hoechst stains nuclear DNA (blue), and phalloidin stains F-actin (violet).

(K) Proportion of cells displaying preferential nuclear (N), nuclear and cytoplasmic (N/C), or cytoplasmic (C) YAP location (left panel; n = 50–100 cells).

(L) Y-27632 or Lat.A treatments were followed by western blot analysis for p-cofilin, cofilin, p127-YAP, YAP, and α tubulin as a loading control.

(M) Impact of Y-27632 and Lat.A treatments on the expression of endogenous YAP-regulated genes (*CTGF* and *CYR61*) in OMM1.3 and OMM1.5 uveal melanoma cells (mean ± SEM, n = 3).

See also Figure S3.

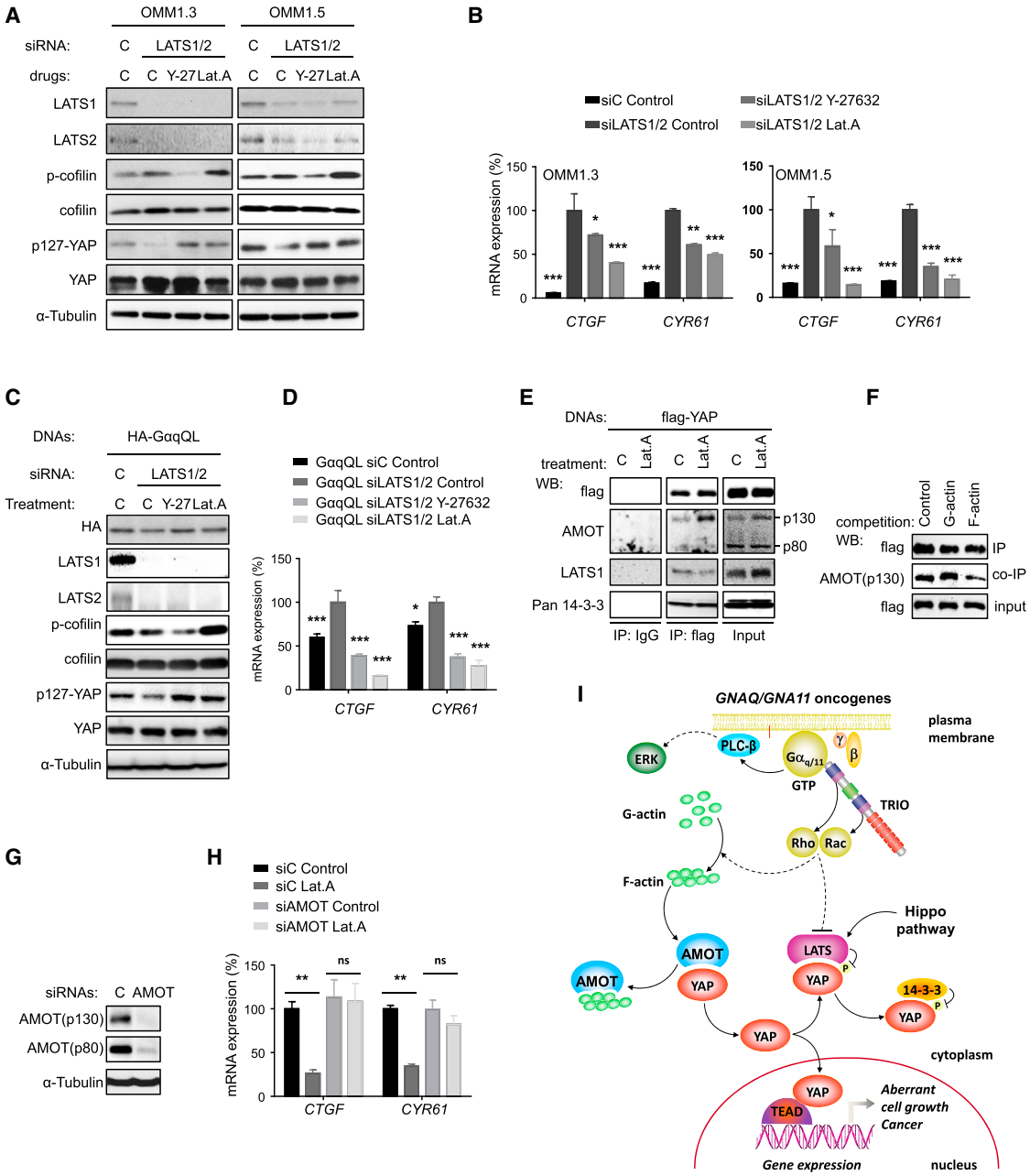

Figure 5. Actin Remodeling Results in Hippo-Independent Activation of YAP Downstream of *GNAQ* Oncogenic Signaling

(A) OMM1.3 and OMM1.5 cells were transfected with siRNAs for LATS1 and LATS2 and treated with control diluent or Y-27632 and Lat.A, followed by western blot analysis for LATS1, LATS2, p-cofilin, cofilin, p127-YAP, YAP, and α tubulin as a loading control.

(B) Similarly, cells were also followed by qPCR to analyze the expression of YAP-regulated genes (*CTGF* and *CYR61*) (mean ± SEM, n = 3).

(C) HEK293 cells were cotransfected with siRNA, LATS1 and LATS2, and HA-GαqQL and treated with Y-27632 or Lat.A, followed by the indicated western blot analysis for HA-GαqQL, LATS1, LATS2, p-cofilin, cofilin, p127-YAP, YAP, and α tubulin as a loading control.

(D) Cells were also followed by qPCR to assess the expression levels of YAP-regulated genes (*CTGF* and *CYR61*) (mean ± SEM, n = 3).

(E) OMM1.3 cells expressing flag-tagged YAP treated with Lat.A or control were lysed and followed by antiflag and control (immunoglobulin G) IP and western blot analysis for flag-YAP, AMOT, LATS1, and 14-3-3 present in the immunoprecipitates, using the input lysate as control.

(F) Antiflag immunoprecipitates from HEK293 cells expressing flag-YAP were exposed to G-actin or F-actin, washed, and analyzed by western blot for flag-YAP and associated endogenous AMOT.

(G) OMM1.3 cells were transfected with siRNA for AMOT, followed by the indicated western blot analysis for AMOT (recognizing both p130 and p80 forms) and α tubulin as a loading control.

(H) OMM1.3 cells were transfected with siRNA AMOT or siRNA control, followed by Lat.A treatment or control, and the expression of YAP-regulated genes (*CTGF* and *CYR61*) was determined by qPCR.

(legend continued on next page)

for cell movement, they both converge in the activation of LIMK and the consequent phosphorylation and inactivation of the actin-severing protein cofilin, thus favoring actin polymerization and F-actin accumulation (reviewed in Bar-Sagi and Hall, 2000). RhoA activates LIMK through ROCK, and Rac1 stimulates this kinase through PAK (reviewed in Bar-Sagi and Hall, 2000; Radu et al., 2014), which can explain why ROCK inhibitors do not prevent the activation of YAP by the latter. In turn, how F-actin stimulates YAP was unclear (reviewed in Matsui and Lai, 2013). YAP is part of multiple cytosolic protein complexes, many of which are driven by the direct interaction between the WW domains of YAP with the PPxY motifs present in most of its associated proteins, including LATS and AMOT (Sudol, 2013; Sudol et al., 2012; Wang et al., 2014). The latter has recently received increased attention, as AMOT represses YAP function (Chan et al., 2011; Zhao et al., 2011) and competes for LATS binding to YAP (Yi et al., 2013), while there are no AMOT orthologs in *Drosophila*, thus representing a fundamental difference in Hippo signaling between *Drosophila* and vertebrates (Bossuyt et al., 2014). Our present findings are consistent with a model in which AMOT retains YAP in a complex that is protected from LATS inhibition, but this AMOT-bound pool of YAP can then be mobilized by F-actin, promoting the release of YAP and its subsequent nuclear accumulation, resulting in increased transcription of its target genes (Figure 5I). In turn, this potential mechanism of YAP regulation may explain the still poorly understood mechanosensing role of YAP and some seemingly contradictory results regarding AMOT function, as AMOT may act as a YAP inhibitor or facilitate YAP activation depending on the status of actin polymerization. These possibilities, as well as how the interplay between AMOT and LATS and the actin cytoskeleton (Adler et al., 2013; Chan et al., 2013; Dai et al., 2013; Hong, 2013; Paramasivam et al., 2011; Yi et al., 2013) regulates YAP, will surely warrant further investigation.

A high rate of mutations in GPCRs and G proteins has been recently identified in melanoma (Kan et al., 2010; O'Hayre et al., 2013; Prickett et al., 2011). Strikingly, mutations in *GNAQ* and *GNA11* have been observed in the majority of uveal melanomas, 83% of blue nevi, 6% of cutaneous melanomas, and 59% of tumors arising in the meninges (Küsters-Vandevelde et al., 2010; Van Raamsdonk et al., 2009). Somatic mosaic mutations in *GNAQ* have been also recently identified in port-wine stains in infants and as the genetic alteration underlying Sturge-Weber syndrome (Shirley et al., 2013), while *GNA11* gain-of-function mutations cause autosomal-dominant hypocalcemia (Nesbit et al., 2013). The growth-promoting potential of *GNAQ* mutants requires the activation of a complex signaling network stimulating the expression of AP-1-regulated genes (Vaqué et al., 2013). However, this signaling route may not yet be suitable for cancer treatment. Here, we show that activation of YAP represents a key molecular event downstream of *GNAQ* and *GNA11* in uveal melanoma. Moreover, recent efforts have exposed YAP as a suitable therapeutic target (Sudol et al., 2012). Liu-Chittenden et al. (2012) screened a small-molecule library for compounds inhibiting the transcriptional activity of YAP in vitro. Among them, VP, a benzoporphyrin derivative, is in clinical use as a photosensitizer in photocoagulation therapy for patients with wet age-related macular degeneration (Michels and Schmidt-Erfurth, 2001). Both YAP knockdown and VP treatment reduce uveal melanoma cell growth in vitro and tumor formation in vivo. In light of our observations, the successful use of photodynamic therapy (PDT) using VP as a photosensitizer for the treatment of some patients with posterior uveal melanomas (Barbazetto et al., 2003; Soucek and Cihelkova, 2006) is very intriguing. It is presumed that the mechanism of action of PDT for uveal melanoma is damage to the tumor vasculature, but the pharmacological inhibition of YAP by VP may provide an unexpected alternative explanation for its therapeutic success in some patients. Indeed, although it is unclear whether VP may be also active in cancers driven by other tumor-promoting genes, we can postulate that the transcriptional coactivator YAP may represent a suitable therapeutic target for the treatment of uveal melanoma and other human diseases that result from gain-of-function mutations in the *GNAQ* and *GNA11* oncogenes.

EXPERIMENTAL PROCEDURES

Cell Lines, Culture Procedures, and Chemicals

Uveal melanoma OMM1.3, OMM1.5, Mel270, and 92.1 cells and cutaneous melanoma WM-266 and SK-mel-2 cells have been described elsewhere (Schmitt et al., 2007; Zuidervaart et al., 2005). Cells knocked down for Trio and YAP and their corresponding controls were generated as described in Supplemental Experimental Procedures. Y-27632 (Tocris Cookson) (10 μM) and Lat.A (Tocris Cookson) (1 μM) were used to treat uveal melanoma cells for 1 or 6 h, followed by immunofluorescence, western blot analysis and immunoprecipitation (IP) or quantitative PCR (qPCR), respectively. VP (Chemical Abstracts Service No. 129497-78-5; USP Reference Standards) was prepared as a stock solution in DMSO. See Supplemental Experimental Procedures.

Small Interfering RNA and DNA Constructs

All human small interfering RNA (siRNA) sequences and providers, as well as DNA constructs, are described in Supplemental Experimental Procedures.

Statistical Analysis

All data analysis was performed using GraphPad Prism version 6 for Windows (GraphPad Software). The data were analyzed using ANOVA or t tests.

Animal Studies

All animal studies were approved by the Animal Care and Use Committee, National Institute of Dental and Craniofacial Research, in compliance with

(I) Schematic representation of Hippo-dependent and Hippo-independent pathways resulting in YAP activation by the *GNAQ* oncogene in uveal melanoma. Gαq protein stimulates YAP through a RhoA and Rac1 regulated signaling circuitry initiated by the activation of Trio, a Rho-GEF activating these GTPases, independently of the best-known stimulation of second messengers through PLCβ. In turn, RhoA activates ROCK and Rac1 stimulates PAK proteins, which converge in the activation of LIMK that phosphorylates and inactivates the actin-severing protein cofilin, resulting in actin polymerization and F-actin accumulation (not depicted for simplicity, dotted line). F-actin may then bind AMOT, displacing YAP, which translocates to the nucleus and initiates gene expression. Free YAP can also bind to LATS, which phosphorylates and inactivates YAP upon the cytosolic sequestration of phospho-YAP by 14-3-3 proteins or by promoting its proteosomal degradation (the latter not depicted), as part of a canonical Hippo-dependent pathway restraining YAP function. How Rho GTPases regulate LATS function is not fully understood (dotted line). It is expected that in the presence of *GNAQ* oncogenes, LATS reduced activity acts in a coordinated function with the likely dominant F-actin-mediated stimulation of YAP to promote YAP stabilization and nuclear translocation, ultimately resulting in the expression of YAP-regulated growth-promoting genes. See text for details.

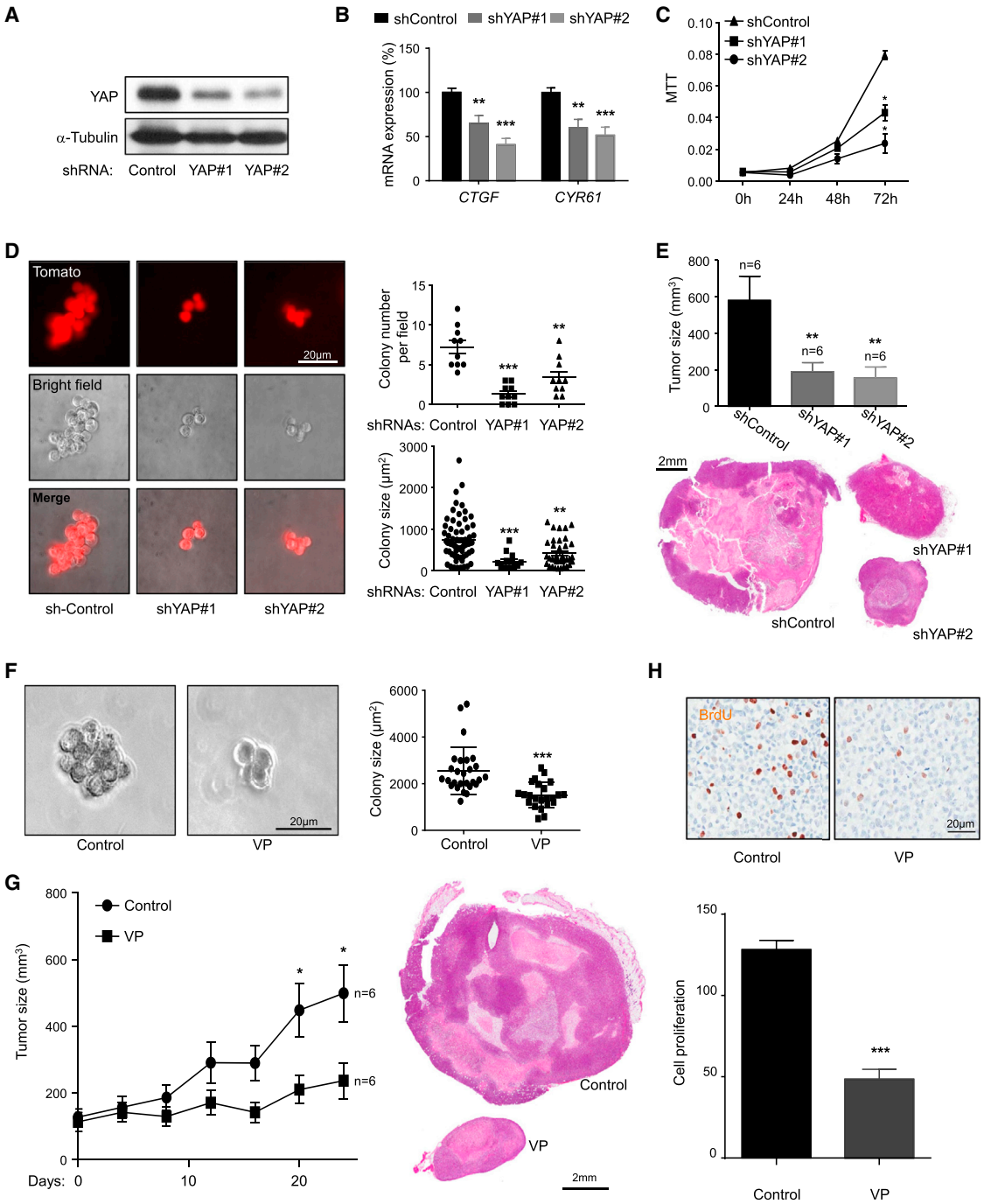

Figure 6. YAP Represents a Therapeutic Target in Uveal Melanoma

(A) Western blot shows YAP knockdown by doxycycline-inducible shRNAs (YAP#1 and YAP#2) in OMM1.3 uveal melanoma cells.

(B) Impact of shRNAs knocking down YAP on the expression of endogenous YAP-regulated genes (*CTGF* and *CYR61*) in OMM1.3 uveal melanoma cells (mean ± SEM, n = 5).

(C) Effect of shRNA knock down of YAP in OMM1.3 uveal melanoma cell proliferation (mean ± SEM, n = 3).

(D) OMM1.3 uveal melanoma cell colony formation in soft agar after shRNA-mediated knockdown of YAP. shRNA positive cells (control and YAP#1 and YAP#2) expressed Tomato (red) (left panel), nd were counted (right upper panel) (mean ± SEM, n = 10) and their size measured (right lower panel) with ImageJ (mean ± SEM, n = 20–100 colonies).

(E) OMM1.3 uveal melanoma formation in vivo in cells expressing control and YAP shRNAs. Tumor size at the end of the study was measured (mean ± SEM, n = 6) (upper panel); hematoxylin and eosin (H&E)-stained sections of representative tumors from each group are shown (lower panel).

(F) Soft agar assays show the effect of VP treatment on OMM1.3 uveal melanoma cell colony formation ability (left panel) and colony size (mean ± SEM, n = 20–50 colonies) (right panel).

(legend continued on next page)

the *Guide for the Care and Use of Laboratory Animals*. Animals were housed on 12-h light/dark cycles and received food, standard rodent chow, and water ad libitum in compliance with Association for Assessment and Accreditation of Laboratory Animal Care International guidelines. See also Supplemental Experimental Procedures.

Human Tumor Xenografts and In Vivo Treatment with VP

Female NOD.Cg-*Prkdc*^{scid} *Il2rgt*^{m1wjl}/SzJ mice 5 to 6 weeks of age weighing 18 to 20 g were used in the study of tumor formation essentially as previously described (Vaqué et al., 2013). The animals were monitored twice weekly for tumor development. Results of animal experiments were expressed as mean ± SEM of a total of six tumors analyzed. See Supplemental Experimental Procedures for technical details and a description of the treatment with VP (Liu-Chittenden et al., 2012).

Small GTPase Activation, Immunobloting, and Phosphoinositide Turnover Assays

RhoA and Rac1 activity was assessed using a modified method described previously (Vaqué et al., 2013). Western blots and phosphoinositide (PI) turnover assays were performed as described previously (Vaqué et al., 2013). See Supplemental Experimental Procedures for antibody information and technical details.

IP and YAP-Protein Complex Interaction and Competition Assays

See Supplemental Experimental Procedures.

Clinical Samples

Snap-frozen uveal melanoma tissues were generously provided by Dr. James T. Handa and Dr. Shannath Merbs, Wilmer Eye Institute, Johns Hopkins School of Medicine; tissue was obtained from consenting patients in accordance with a study approved by the Institutional Review Board at the Johns Hopkins School of Medicine. Normal skin samples were purchased from US Biomax and Biochain.

Immunofluorescence

See Supplemental Experimental Procedures.

Luciferase Assays

HEK293 cells were cotransfected with TEAD4-Gal4 (0.5 μg/ml), Gal4-luc (0.5 μg/ml), and pRLNull (1 μg/ml) in 24-well plates overnight to the detection of the luciferase activity, using a Dual-Glo Luciferase Assay Kit (Promega) and a Microtiter plate luminometer (Dynex Technologies).

Immunohistochemistry

See Supplemental Experimental Procedures.

Growth in Soft Agar

Cells were mixed at a concentration of 2,500 cells/0.2 ml of medium, and 0.2% agar (Lonza). The cells in 0.2% agar were plated over 0.2 ml of medium, 1% agar that had been allowed to harden in a 96-well dish. Cells were fed 50 μl of medium every 4 days. In the VP treatment assay, VP was added in the medium with a final concentration of 1 μM.

Nuclear and Cytoplasm Extraction

Follow the instructions of NE-PER Nuclear and Cytoplasmic Extraction Reagents (Thermo Fisher Scientific).

SUPPLEMENTAL INFORMATION

Supplemental Information includes Supplemental Experimental Procedures and three figures and can be found with this article online at http://dx.doi.org/10.1016/j.ccr.2014.04.016.

ACKNOWLEDGMENTS

We acknowledge the extensive support, guidance, and help from all members of the J.S.G. laboratory and the Oral Cancer Branch for their generous contributions and thoughtful suggestions throughout these studies. We thank Dr. Thomas Bugge and Dr. Marius Sudol for insightful advice and critically reading our manuscript. We thank Dr. James T. Handa and Dr. Shannath Merbs, Wilmer Eye Institute, Johns Hopkins School of Medicine, for generously providing snap-frozen uveal melanoma tissue. This research was partially supported by the Intramural Research Program of NIH, National Institute of Dental and Craniofacial Research. We apologize to all of our colleagues for not citing some of their original studies because of space limitations.

Received: October 19, 2013
Revised: March 6, 2014
Accepted: April 24, 2014
Published: May 29, 2014

REFERENCES

Adler, J.J., Johnson, D.E., Heller, B.L., Bringman, L.R., Ranahan, W.P., Conwell, M.D., Sun, Y., Hudmon, A., and Wells, C.D. (2013). Serum deprivation inhibits the transcriptional co-activator YAP and cell growth via phosphorylation of the 130-kDa isoform of Angiomotin by the LATS1/2 protein kinases. Proc. Natl. Acad. Sci. U S A *110*, 17368–17373.

Aragona, M., Panciera, T., Manfrin, A., Giulitti, S., Michielin, F., Elvassore, N., Dupont, S., and Piccolo, S. (2013). A mechanical checkpoint controls multicellular growth through YAP/TAZ regulation by actin-processing factors. Cell *154*, 1047–1059.

Barbazetto, I.A., Lee, T.C., Rollins, I.S., Chang, S., and Abramson, D.H. (2003). Treatment of choroidal melanoma using photodynamic therapy. Am. J. Ophthalmol. *135*, 898–899.

Bar-Sagi, D., and Hall, A. (2000). Ras and Rho GTPases: a family reunion. Cell *103*, 227–238.

Berman, D.M., Wilkie, T.M., and Gilman, A.G. (1996). GAIP and RGS4 are GTPase-activating proteins for the Gi subfamily of G protein alpha subunits. Cell *86*, 445–452.

Bernard, O. (2007). Lim kinases, regulators of actin dynamics. Int. J. Biochem. Cell Biol. *39*, 1071–1076.

Bossuyt, W., Chen, C.L., Chen, Q., Sudol, M., McNeill, H., Pan, D., Kopp, A., and Halder, G. (2014). An evolutionary shift in the regulation of the Hippo pathway between mice and flies. Oncogene *33*, 1218–1228.

Camargo, F.D., Gokhale, S., Johnnidis, J.B., Fu, D., Bell, G.W., Jaenisch, R., and Brummelkamp, T.R. (2007). YAP1 increases organ size and expands undifferentiated progenitor cells. Curr. Biol. *17*, 2054–2060.

Castellano, M., Pollock, P.M., Walters, M.K., Sparrow, L.E., Down, L.M., Gabrielli, B.G., Parsons, P.G., and Hayward, N.K. (1997). CDKN2A/p16 is inactivated in most melanoma cell lines. Cancer Res. *57*, 4868–4875.

Chan, S.W., Lim, C.J., Chong, Y.F., Pobbati, A.V., Huang, C., and Hong, W. (2011). Hippo pathway-independent restriction of TAZ and YAP by angiomotin. J. Biol. Chem. *286*, 7018–7026.

Chan, S.W., Lim, C.J., Guo, F., Tan, I., Leung, T., and Hong, W. (2013). Actin-binding and cell proliferation activities of angiomotin family members are regulated by Hippo pathway-mediated phosphorylation. J. Biol. Chem. *288*, 37296–37307.

Dai, X., She, P., Chi, F., Feng, Y., Liu, H., Jin, D., Zhao, Y., Guo, X., Jiang, D., Guan, K.L., et al. (2013). Phosphorylation of angiomotin by Lats1/2 kinases inhibits F-actin binding, cell migration, and angiogenesis. J. Biol. Chem. *288*, 34041–34051.

(G) Effect of VP on OMM1.3 uveal melanoma cell growth in vivo. Tumor size was measured every 4 days after the initiation of the VP treatment and control (mean ± SEM, n = 6; n = number of tumors analyzed) (left panel). H&E-stained sections of representative tumors from each group (right panels).
(H) Effect of VP treatment on OMM1.3 uveal melanoma cell proliferation in the tumor in vivo. Immunohistochemistry staining targeting Brdu in OMM1.3 tumors shows Brdu-positive cells (upper panel), which were quantified in multiple tumor sections (mean ± SEM, n = 20) (lower panel).

Dong, J., Feldmann, G., Huang, J., Wu, S., Zhang, N., Comerford, S.A., Gayyed, M.F., Anders, R.A., Maitra, A., and Pan, D. (2007). Elucidation of a universal size-control mechanism in Drosophila and mammals. Cell *130*, 1120–1133.

Dupont, S., Morsut, L., Aragona, M., Enzo, E., Giulitti, S., Cordenonsi, M., Zanconato, F., Le Digabel, J., Forcato, M., Bicciato, S., et al. (2011). Role of YAP/TAZ in mechanotransduction. Nature *474*, 179–183.

Griner, E.M., and Kazanietz, M.G. (2007). Protein kinase C and other diacylglycerol effectors in cancer. Nat. Rev. Cancer *7*, 281–294.

Halder, G., Dupont, S., and Piccolo, S. (2012). Transduction of mechanical and cytoskeletal cues by YAP and TAZ. Nat. Rev. Mol. Cell Biol. *13*, 591–600.

Hong, W. (2013). Angiomotin'g YAP into the nucleus for cell proliferation and cancer development. Sci. Signal. *6*, pe27.

Hubbard, K.B., and Hepler, J.R. (2006). Cell signalling diversity of the Gqalpha family of heterotrimeric G proteins. Cell. Signal. *18*, 135–150.

Johnson, R., and Halder, G. (2014). The two faces of Hippo: targeting the Hippo pathway for regenerative medicine and cancer treatment. Nat. Rev. Drug Discov. *13*, 63–79.

Kan, Z., Jaiswal, B.S., Stinson, J., Janakiraman, V., Bhatt, D., Stern, H.M., Yue, P., Haverty, P.M., Bourgon, R., Zheng, J., et al. (2010). Diverse somatic mutation patterns and pathway alterations in human cancers. Nature *466*, 869–873.

Küsters-Vandevelde, H.V., Klaasen, A., Küsters, B., Groenen, P.J., van Engen-van Grunsven, I.A., van Dijk, M.R., Reifenberger, G., Wesseling, P., and Blokx, W.A. (2010). Activating mutations of the GNAQ gene: a frequent event in primary melanocytic neoplasms of the central nervous system. Acta Neuropathol. *119*, 317–323.

Liu-Chittenden, Y., Huang, B., Shim, J.S., Chen, Q., Lee, S.J., Anders, R.A., Liu, J.O., and Pan, D.J. (2012). Genetic and pharmacological disruption of the TEAD-YAP complex suppresses the oncogenic activity of YAP. Genes Dev. *26*, 1300–1305.

Matsui, Y., and Lai, Z.C. (2013). Mutual regulation between Hippo signaling and actin cytoskeleton. Protein Cell *4*, 904–910.

Michels, S., and Schmidt-Erfurth, U. (2001). Photodynamic therapy with verteporfin: a new treatment in ophthalmology. Semin. Ophthalmol. *16*, 201–206.

Mo, J.S., Yu, F.X., Gong, R., Brown, J.H., and Guan, K.L. (2012). Regulation of the Hippo-YAP pathway by protease-activated receptors (PARs). Genes Dev. *26*, 2138–2143.

Mohseni, M., Sun, J., Lau, A., Curtis, S., Goldsmith, J., Fox, V.L., Wei, C., Frazier, M., Samson, O., Wong, K.K., et al. (2014). A genetic screen identifies an LKB1-MARK signalling axis controlling the Hippo-YAP pathway. Nat. Cell Biol. *16*, 108–117.

Nesbit, M.A., Hannan, F.M., Howles, S.A., Babinsky, V.N., Head, R.A., Cranston, T., Rust, N., Hobbs, M.R., Heath, H., 3rd, and Thakker, R.V. (2013). Mutations affecting G-protein subunit α11 in hypercalcemia and hypocalcemia. N. Engl. J. Med. *368*, 2476–2486.

O'Hayre, M., Vázquez-Prado, J., Kufareva, I., Stawiski, E.W., Handel, T.M., Seshagiri, S., and Gutkind, J.S. (2013). The emerging mutational landscape of G proteins and G-protein-coupled receptors in cancer. Nat. Rev. Cancer *13*, 412–424.

Oka, T., Schmitt, A.P., and Sudol, M. (2012). Opposing roles of angiomotin-like-1 and zona occludens-2 on pro-apoptotic function of YAP. Oncogene *31*, 128–134.

Pan, D.J. (2010). The hippo signaling pathway in development and cancer. Dev. Cell *19*, 491–505.

Paramasivam, M., Sarkeshik, A., Yates, J.R., 3rd, Fernandes, M.J., and McCollum, D. (2011). Angiomotin family proteins are novel activators of the LATS2 kinase tumor suppressor. Mol. Biol. Cell *22*, 3725–3733.

Pollard, T.D., and Cooper, J.A. (2009). Actin, a central player in cell shape and movement. Science *326*, 1208–1212.

Prickett, T.D., Wei, X., Cardenas-Navia, I., Teer, J.K., Lin, J.C., Walia, V., Gartner, J., Jiang, J., Cherukuri, P.F., Molinolo, A., et al. (2011). Exon capture analysis of G protein-coupled receptors identifies activating mutations in GRM3 in melanoma. Nat. Genet. *43*, 1119–1126.

Radu, M., Semenova, G., Kosoff, R., and Chernoff, J. (2014). PAK signalling during the development and progression of cancer. Nat. Rev. Cancer *14*, 13–25.

Ramos, A., and Camargo, F.D. (2012). The Hippo signaling pathway and stem cell biology. Trends Cell Biol. *22*, 339–346.

Schlegelmilch, K., Mohseni, M., Kirak, O., Pruszak, J., Rodriguez, J.R., Zhou, D., Kreger, B.T., Vasioukhin, V., Avruch, J., Brummelkamp, T.R., and Camargo, F.D. (2011). Yap1 acts downstream of α-catenin to control epidermal proliferation. Cell *144*, 782–795.

Schmitt, C.J., Franke, W.W., Goerdt, S., Falkowska-Hansen, B., Rickelt, S., and Peitsch, W.K. (2007). Homo- and heterotypic cell contacts in malignant melanoma cells and desmoglein 2 as a novel solitary surface glycoprotein. J. Invest. Dermatol. *127*, 2191–2206.

Shirley, M.D., Tang, H., Gallione, C.J., Baugher, J.D., Frelin, L.P., Cohen, B., North, P.E., Marchuk, D.A., Comi, A.M., and Pevsner, J. (2013). Sturge-Weber syndrome and port-wine stains caused by somatic mutation in GNAQ. N. Engl. J. Med. *368*, 1971–1979.

Soucek, P., and Cihelkova, I. (2006). Photodynamic therapy with verteporfin in subfoveal amelanotic choroidal melanoma (A controlled case). Neuroendocrinol. Lett. *27*, 145–148.

Sudol, M. (2013). YAP1 oncogene and its eight isoforms. Oncogene *32*, 3922.

Sudol, M., Bork, P., Einbond, A., Kastury, K., Druck, T., Negrini, M., Huebner, K., and Lehman, D. (1995). Characterization of the mammalian YAP (Yes-associated protein) gene and its role in defining a novel protein module, the WW domain. J. Biol. Chem. *270*, 14733–14741.

Sudol, M., Shields, D.C., and Farooq, A. (2012). Structures of YAP protein domains reveal promising targets for development of new cancer drugs. Semin. Cell Dev. Biol. *23*, 827–833.

van der Velden, P.A., Metzelaar-Blok, J.A., Bergman, W., Monique, H., Hurks, H., Frants, R.R., Gruis, N.A., and Jager, M.J. (2001). Promoter hypermethylation: a common cause of reduced p16(INK4a) expression in uveal melanoma. Cancer Res. *61*, 5303–5306.

Van Raamsdonk, C.D., Bezrookove, V., Green, G., Bauer, J., Gaugler, L., O'Brien, J.M., Simpson, E.M., Barsh, G.S., and Bastian, B.C. (2009). Frequent somatic mutations of GNAQ in uveal melanoma and blue naevi. Nature *457*, 599–602.

Van Raamsdonk, C.D., Griewank, K.G., Crosby, M.B., Garrido, M.C., Vemula, S., Wiesner, T., Obenauf, A.C., Wackernagel, W., Green, G., Bouvier, N., et al. (2010). Mutations in GNA11 in uveal melanoma. N. Engl. J. Med. *363*, 2191–2199.

Vaqué, J.P., Dorsam, R.T., Feng, X.D., Iglesias-Bartolome, R., Forsthoefel, D.J., Chen, Q.M., Debant, A., Seeger, M.A., Ksander, B.R., Teramoto, H., and Gutkind, J.S. (2013). A genome-wide RNAi screen reveals a Trio-regulated Rho GTPase circuitry transducing mitogenic signals initiated by G protein-coupled receptors. Mol. Cell *49*, 94–108.

Vitale-Cross, L., Amornphimoltham, P., Fisher, G., Molinolo, A.A., and Gutkind, J.S. (2004). Conditional expression of K-ras in an epithelial compartment that includes the stem cells is sufficient to promote squamous cell carcinogenesis. Cancer Res. *64*, 8804–8807.

Wang, W., Li, X., Huang, J., Feng, L., Dolinta, K.G., and Chen, J. (2014). Defining the protein-protein interaction network of the human hippo pathway. Mol. Cell. Proteomics *13*, 119–131.

Yi, C., Shen, Z., Stemmer-Rachamimov, A., Dawany, N., Troutman, S., Showe, L.C., Liu, Q., Shimono, A., Sudol, M., Holmgren, L., et al. (2013). The p130 isoform of angiomotin is required for Yap-mediated hepatic epithelial cell proliferation and tumorigenesis. Sci. Signal. *6*, ra77.

Yin, F., Yu, J., Zheng, Y., Chen, Q., Zhang, N., and Pan, D. (2013). Spatial organization of Hippo signaling at the plasma membrane mediated by the tumor suppressor Merlin/NF2. Cell *154*, 1342–1355.

Yu, F.X., Zhao, B., Panupinthu, N., Jewell, J.L., Lian, I., Wang, L.H., Zhao, J.G., Yuan, H.X., Tumaneng, K., Li, H.R., et al. (2012). Regulation of the Hippo-YAP pathway by G-protein-coupled receptor signaling. Cell *150*, 780–791.

Zaidi, M.R., Davis, S., Noonan, F.P., Graff-Cherry, C., Hawley, T.S., Walker, R.L., Feigenbaum, L., Fuchs, E., Lyakh, L., Young, H.A., et al. (2011). Interferon-γ links ultraviolet radiation to melanomagenesis in mice. Nature *469*, 548–553.

Zhao, B., Wei, X., Li, W., Udan, R.S., Yang, Q., Kim, J., Xie, J., Ikenoue, T., Yu, J., Li, L., et al. (2007). Inactivation of YAP oncoprotein by the Hippo pathway is involved in cell contact inhibition and tissue growth control. Genes Dev. *21*, 2747–2761.

Zhao, B., Li, L., Lei, Q., and Guan, K.L. (2010). The Hippo-YAP pathway in organ size control and tumorigenesis: an updated version. Genes Dev. *24*, 862–874.

Zhao, B., Li, L., Lu, Q., Wang, L.H., Liu, C.Y., Lei, Q., and Guan, K.L. (2011). Angiomotin is a novel Hippo pathway component that inhibits YAP oncoprotein. Genes Dev. *25*, 51–63.

Zuidervaart, W., van Nieuwpoort, F., Stark, M., Dijkman, R., Packer, L., Borgstein, A.M., Pavey, S., van der Velden, P., Out, C., Jager, M.J., et al. (2005). Activation of the MAPK pathway is a common event in uveal melanomas although it rarely occurs through mutation of BRAF or RAS. Br. J. Cancer *92*, 2032–2038.

nature structural & molecular biology

Allosteric enhancement of MAP kinase p38α's activity and substrate selectivity by docking interactions

Yuji Tokunaga[1,2], Koh Takeuchi[3], Hideo Takahashi[3,4] & Ichio Shimada[2,3]

Mitogen-activated protein kinases (MAPKs) are essential to intracellular signal transduction. MAPKs anchor their pathway-specific substrates through so-called 'docking interactions' at locations distal from the active site. Docking interactions ensure efficient substrate recognition, but their contribution to the kinase reaction itself remains unclear. Herein, we use solution NMR to analyze the interaction between dually phosphorylated, active human p38α and the C-terminal fragments of its substrate MK2. p38α phosphorylation and ATP loading collaboratively induce the active conformation; subsequently, p38α accommodates MK2 phosphoacceptor residues in its active site. The docking interaction enhances binding of ATP and the phosphoacceptor to p38α, accelerating the phosphotransfer reaction. Thus, the docking interaction enhances p38α's enzymatic activity toward pathway-specific substrates allosterically as well as by the anchor effect. These findings clarify how MAPK cascades are organized in cells, even under ATP-depleted conditions often associated with environmental stress.

MAPKs have pivotal roles in intracellular signal transduction, the process of converting various stimuli into corresponding cellular events[1–5]. An isoform of the p38 subfamily, p38α, mediates stress-induced apoptosis[6] and is involved in the production of inflammatory cytokines, including tumor necrosis factor α, thus making the protein a potential drug target for inflammatory diseases[7,8]. Because of the importance of MAPKs in various cellular functions, MAPK signals must be strictly regulated to elicit the correct cellular responses[1,5]. MAPKs are controlled in a common scheme called the MAPK cascade, which is characterized by the stepwise phosphorylation of three tiers of hierarchical kinases: MAPK kinase kinase, MAPK kinase (MAPKK) and MAPK[9]. The activated MAPKK dually phosphorylates MAPK at the threonine and tyrosine residues in the conserved TXY motif, which is required for the full activation of MAPK[10,11]. The activated MAPK phosphorylates its substrates to evoke cellular responses[3] that are subsequently turned off by their specific phosphatases[12].

MAPKs consist of a typical kinase domain composed of N and C lobes[13–15]. The N lobe binds ATP, and the C lobe contains the P+1 site, to which the substrate's phosphoacceptor residues localize during the phosphotransfer reaction (**Fig. 1a**). An activation loop, which contains the TXY phosphorylation motif (180-TGY-182 for p38α), lies in a groove between these two lobes. Whereas the N and C lobes are spatially separated to form an 'open' conformation in unphosphorylated, inactive MAPKs (for example, PDB 1P38 (ref. 14) and 1WFC[15] for p38α and 1ERK[16] for ERK2), the distance between these two lobes decreases to form a 'closed' conformation in the crystal structure of phosphorylated p38γ bound to adenylyl imidodiphosphate (AMP-PNP; PDB 1CM8 (ref. 17)). Such closure is essential for efficient phosphotransfer because the spatial proximity of the γ-phosphate of ATP, which binds the N lobe, and the hydroxyl groups of the substrate phosphoacceptor residues trapped in the C lobe are a prerequisite for the reaction[17,18]. Crystal structures of phosphorylated apo-MAPKs have been solved in both closed (ERK2, PDB 2ERK[18]) and open (p38α, PDB 3PY3 (ref. 19)) conformations. This suggests that the dual phosphorylation itself may not always coincide with formation of the closed, active conformation of MAPK.

The specific interactions of MAPKs with MAPKKs, substrates and phosphatases rely on conserved docking interactions[20–26] that use sites distal from the active sites in MAPKs and functional sites in the binding partners (for example, the substrate phosphoacceptor sites). In the case of a p38α substrate, MAP kinase–activated protein kinase 2 (MK2), a C-terminal, 30-residue sequence (amino acids (aa) 371–400) is responsible for binding to p38α, while the phosphoacceptor residues, Thr222, Ser272 and Thr334, are distant from the docking sequence (**Fig. 1b**). Deletion of the C-terminal docking sequence in MK2 impairs binding and efficient phosphorylation by p38α (ref. 27). The p38α crystal structures solved in complex with various docking sequences indicate that p38α accommodates the docking sequences in a site located opposite to its active site[28,29] (**Fig. 1a**), and differences in the amino acid compositions of the docking sequences determine the specificity toward the partner molecules[22,30,31]. Therefore, the docking interaction is the key mechanism through which the MAPKs efficiently discriminate their binding partners from the other proteins within the same signaling pathway.

The consensus motif of the MAPK substrate phosphoacceptor site contains serine or threonine followed by proline at the +1 position and a preference for proline at −2. This simple motif overlaps with the phosphorylation motifs of other kinases[32] and thus is not sufficient to

[1]Research and Development Department, Japan Biological Informatics Consortium, Tokyo, Japan. [2]Graduate School of Pharmaceutical Sciences, University of Tokyo, Tokyo, Japan. [3]Biomedicinal Information Research Center, National Institute of Advanced Industrial Science and Technology, Tokyo, Japan. [4]Graduate School of Medical Life Science, Yokohama City University, Kanagawa, Japan. Correspondence should be addressed to I.S. (shimada@iw-nmr.f.u-tokyo.ac.jp).

Received 26 February; accepted 19 June; published online 20 July 2014; doi:10.1038/nsmb.2861

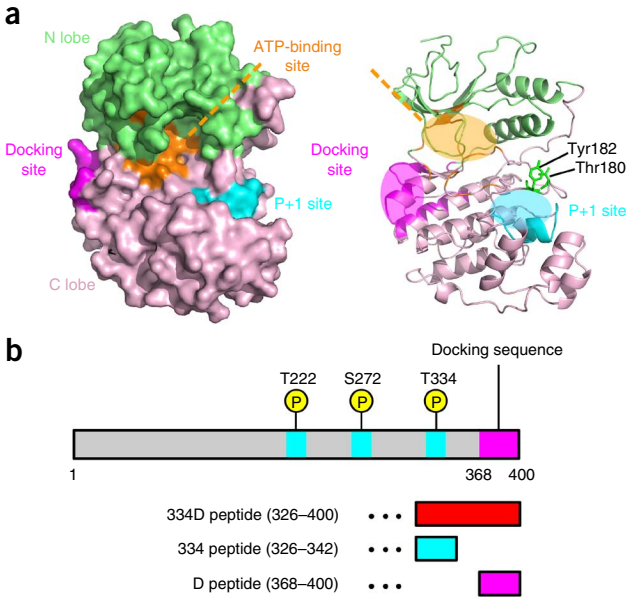

Figure 1 Functional sites in p38α and the substrate peptides used in this study. (**a**) Surface (left) and ribbon (right) representations of a model structure of the dually phosphorylated p38α. The model was generated by the SWISS-MODEL server[50], with the crystal structure of p38γ-2P in complex with AMP-PNP (PDB 1CM8 (ref. 17)) as the template. The structure of bound AMP-PNP was omitted in the figure. The N and C lobes are colored green and pink, respectively. At right, Thr180 and Tyr182 in the activation loop, which are phosphorylated by MAPKK, are indicated by green stick representations, and the ATP-binding site, the P+1 site and the docking site are indicated by orange, cyan and magenta circles, respectively. (**b**) Schematic representation of the p38α substrate, MK2 and the peptides derived from MK2 used in this study.

determine the target specificities of MAPKs. The structural mechanisms underlying phosphoacceptor binding and phosphotransfer are not well understood. The reported structures for a MAPK in complex with a phosphoacceptor-containing substrate are of unphosphorylated p38α (PDB 2ONL[29] and 2OZA[33]). However, these structures cannot explain the phosphotransfer mechanism because the phosphoacceptor residues of the substrate, MK2, do not bind to the P+1 site of p38α. The absence of the interaction may arise from the use of the unphosphorylated, inactive p38α for the structural analysis. In addition, it is not clear whether the docking interaction is used only to tether the substrate and increase the local concentration of phosphoacceptor sites or whether it has additional allosteric effects on the enzymatic activity of MAPK. A previous kinetic analysis showed that ATP and a substrate, activating transcription factor 2 (ATF2), cooperatively enhance the binding to p38α (ref. 34). Such molecular-level analysis, however, cannot determine whether ATP enhances binding at the docking site, phosphoacceptor binding to the P+1 site or both.

Therefore, in this study, we set out to clarify whether the docking interaction allosterically contributes to p38α activity. For this purpose, we prepared dually phosphorylated, active p38α (p38α-2P) and structurally analyzed its interaction with C-terminal fragments of MK2 containing both the docking sequence and the phosphoacceptor residue by solution NMR spectroscopy. We found that all of the individual steps in the p38α-2P kinase reaction, namely binding of ATP and phosphoacceptor residues to the p38α active site and subsequent phosphotransfer, are positively regulated by the docking interaction. Our findings clarify how MAPKs transduce signals steadily in the cell in various environments, including ATP-depleted conditions often associated with stresses, while distinguishing their specific substrates from other miscellaneous proteins.

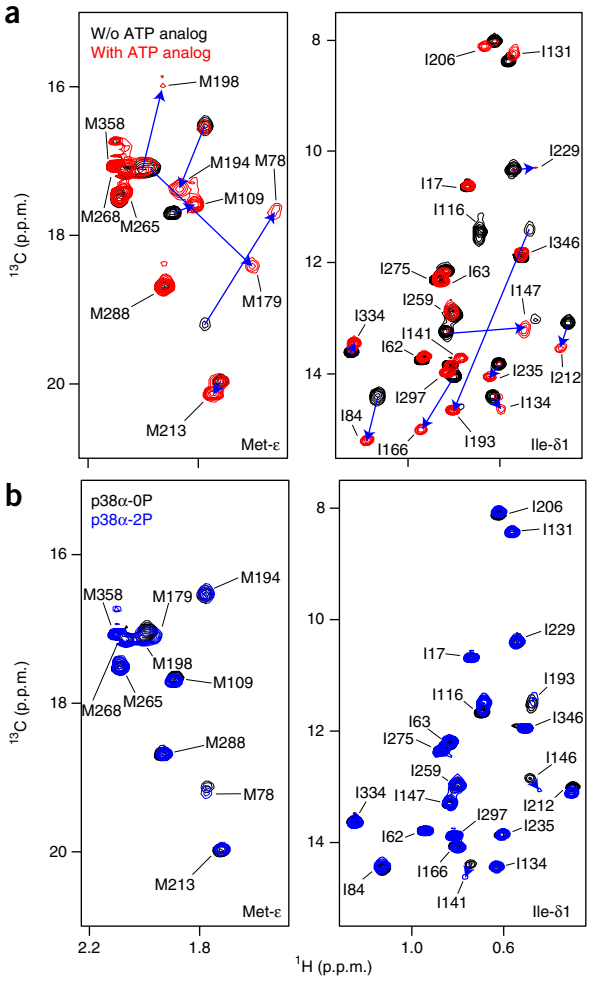

Figure 2 Effects of dual phosphorylation and ATP-analog binding on p38α NMR spectra. (**a**) Overlay of the annotated methionine and isoleucine (δ1) methyl ^{1}H-^{13}C band-selective optimized flip-angle short transient (SOFAST)-HMQC spectra of p38α-2P in the absence (black) and presence (red) of 5 mM ATP analog. Large chemical-shift changes are indicated by blue arrows. (**b**) Overlay of the annotated methionine and isoleucine (δ1) methyl ^{1}H-^{13}C SOFAST-HMQC spectra of p38α-2P (blue) and unphosphorylated p38α (black) in the apo state.

RESULTS

Phosphorylation- and ATP-induced p38α conformational change

As the first step toward gaining insight into the mechanistic regulation of substrate phosphorylation by p38α, we analyzed the phosphorylation- and ATP-dependent activation of p38α. We obtained dually phosphorylated, active p38α-2P by *in vitro* phosphorylation, using a constitutively active form of MAPKK6 (Online Methods and **Supplementary Fig. 1a–k**). p38α-2P in complex with ATP or an ATP analog (ATP-loaded p38α-2P) exhibited substantial chemical-shift perturbations (CSPs) in methyl ^{1}H-^{13}C heteronuclear multiple quantum correlation (HMQC) spectra, as compared to those of apo–p38α-2P (**Fig. 2a** and **Supplementary Fig. 2a**,**b**). Perturbed methyl sites were distributed throughout the structure of p38α and not localized to the ATP-binding site (**Fig. 3a**,**b** and **Supplementary Fig. 2b**), thus indicating

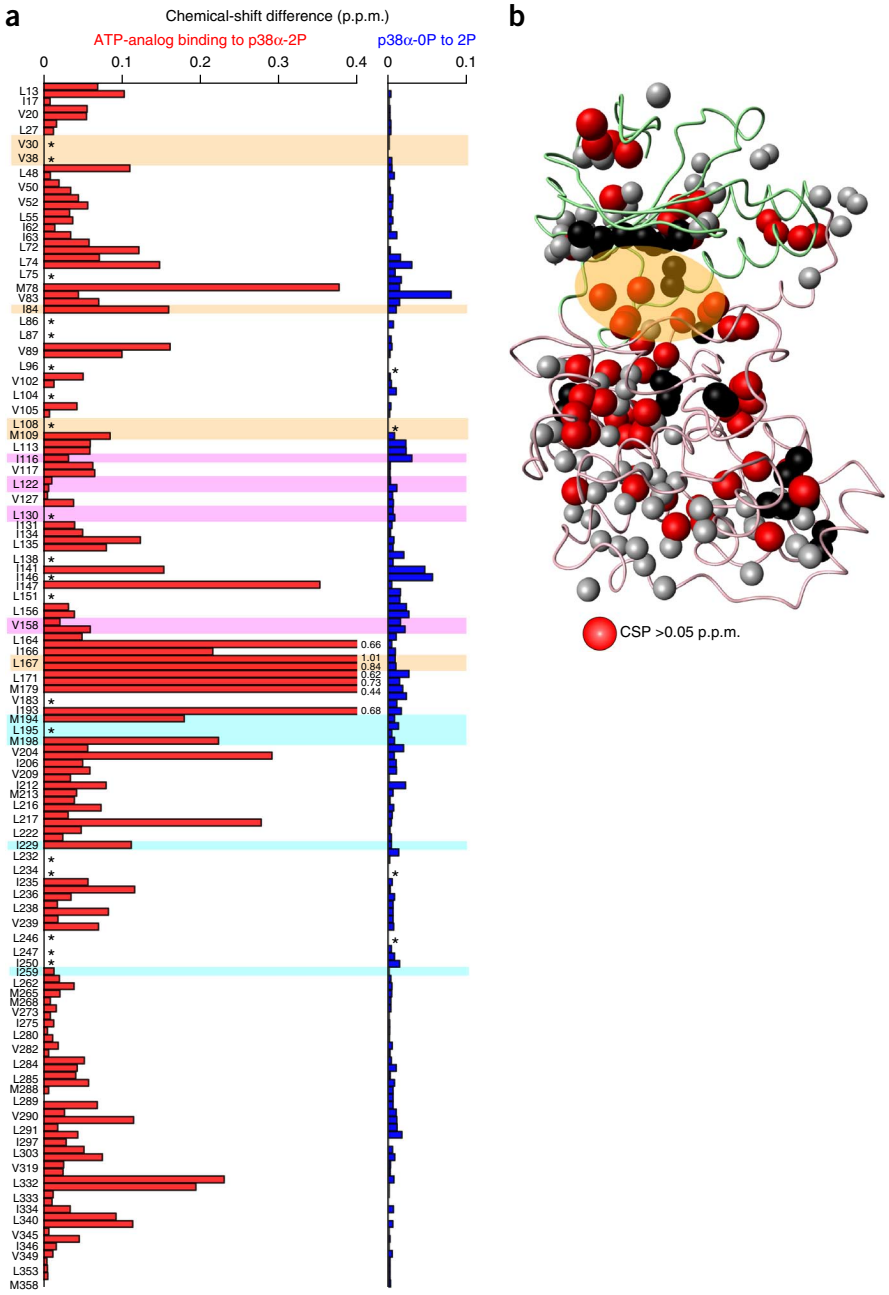

Figure 3 Chemical-shift changes induced by ATP-analog binding to p38α-2P and dual phosphorylation. (**a**) Bar graphs showing the methyl CSPs induced by ATP-analog binding to p38α-2P (left) and the chemical-shift differences between p38α-2P and unphosphorylated p38α (right). The residues in the ATP-binding, docking and P+1 sites are shaded in orange, magenta and cyan, respectively. Unassigned methyl sites are indicated by asterisks. CSP values larger than 0.4 p.p.m. are indicated. For leucine and valine, the values for δ1/γ1 are shown above the values for δ2/γ2. (**b**) Mapping of the CSPs induced by ATP-analog binding to p38α-2P (**a**, left) on the crystal structure of apo-p38α (PDB 1A9U[51]). ILVM-methyl groups are indicated as spheres, and those with CSPs larger than 0.05 p.p.m. are colored red. The ATP-binding site is highlighted by the orange oval. The structure is displayed in the same orientation as in **Figure 1a**.

that p38α underwent a conformational change to the active, closed state upon ATP binding, as observed in the crystal structure of p38γ-2P bound to AMP-PNP[18]. Interestingly, the spectral changes arising from the dual phosphorylation of p38α were smaller than those from ATP binding to p38α-2P (**Figs. 2b** and **3a** and **Supplementary Fig. 2c**). The only change apparent in the p38α spectrum upon dual phosphorylation was the disappearance of the amide ^{1}H-^{15}N resonances originating from the phosphorylated activation loop (aa 179–183), probably because of the conformational multiplicity of this region in the dually phosphorylated state (**Supplementary Fig. 3**). It should also be noted that we observed almost no spectral change for unphosphorylated p38α, even at a high concentration of ATP (4 mM; **Supplementary Fig. 2d**). Thus, both ATP binding and dual phosphorylation are essential to induce an active conformation of p38α-2P, and ATP binding appears to be more important for the overall structural change of p38α-2P, as indicated by the drastic spectral changes upon ATP binding (**Figs. 2** and **3**). In addition, the affinity of unphosphorylated p38α for ATP was quite weak (dissociation constant K_d >15 mM; **Supplementary Fig. 2e**). The size-exclusion chromatography (SEC) data also supported the ATP-dependent closure of p38α-2P, in which the elution volume of p38α-2P in the presence of ATP was larger than that in the absence of ATP (**Supplementary Fig. 1k**).

Substrate binding–induced CSPs in p38α

We next structurally investigated the interactions between the catalytically active, ATP-loaded p38α-2P and the model substrate, a 334D peptide (**Fig. 1b**). The 334D peptide, which contains the C-terminal unstructured region of the p38α substrate MK2, includes a native phosphorylation site, Thr334, and a C-terminal docking sequence. The K_d for 334D-peptide binding to p38α-2P was 80 nM, as determined by isothermal titration calorimetry, a value similar to that previously reported for the longer MK2 fragment (aa 47–400)[27]. Furthermore, the 334D peptide competed with the longer MK2 fragment for binding to p38α-2P (**Supplementary Fig. 1l**) and was phosphorylated more efficiently by p38α-2P than was the 334 peptide (**Supplementary Fig. 1m**), which lacks the docking sequence (**Fig. 1b**). These data confirmed that the 334D peptide retains the characteristics of native p38α substrates.

Titration of the unlabeled 334D peptide to p38α-2P, which was selectively labeled with ^{1}H and ^{13}C at methyl sites of isoleucine (δ1), leucine, valine and methionine (ILVM) residues, induced substantial spectral changes (**Figs. 4** and **5** and **Supplementary Fig. 4**). Resonances from the residues in the docking site, including Ile116 and Val158, exhibited substantial CSPs, both in the absence and presence of the ATP analog (**Fig. 5a–c**). We also observed a large CSP for Met109 in the hinge region, which is located above the docking site (**Fig. 5a–c**). This suggests that anchoring the substrate to p38α-2P via the docking interaction occurs independently of

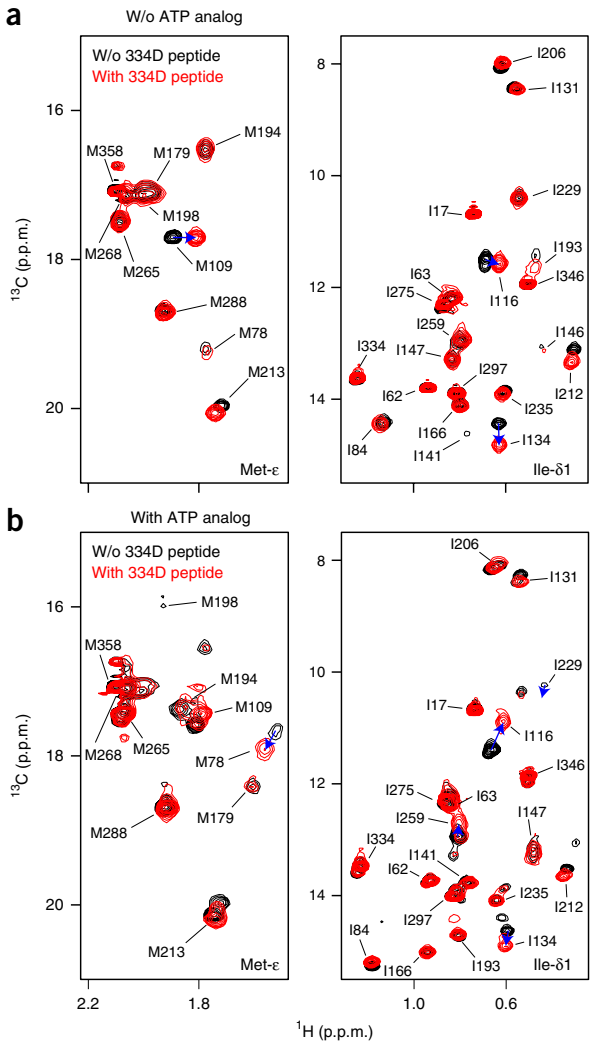

Figure 4 Effects of substrate binding on p38α NMR spectra. (**a**) Overlay of the annotated methionine and isoleucine (δ1) methyl ^{1}H-^{13}C SOFAST-HMQC spectra of p38α-2P without the ATP analog in the absence (black) and presence (red) of an equimolar amount of the 334D peptide. Large chemical-shift changes are indicated by blue arrows. (**b**) As in **a**, except that p38α-2P is in complex with the ATP analog.

ATP-analog binding. The spectral changes were saturated by the addition of an equimolar amount of the 334D peptide, indicating a tight 1:1 stoichiometric interaction between p38α-2P and the MK2 docking sequence (data not shown).

Interestingly, the resonances around the P+1 site showed distinct CSP patterns that were dependent on the presence of the ATP analog (**Fig. 5a–c**). As exemplified by the signals from Met194, Ile229 and Ile259, the P+1 site showed substantial CSPs only in the presence of the ATP analog. When the resonances from the ^{15}N-labeled 334D peptide were observed in the presence of unlabeled p38α-2P, addition of the ATP analog led to the disappearance of the resonances from the 334D peptide, including the resonance from the phosphoacceptor site, Thr334 (**Supplementary Fig. 5a**). These results indicate that the interaction of the 334D peptide with the P+1 site in p38α-2P is formed only upon ATP loading on p38α-2P. This characteristic was not specific to the ATP analog because it was also present for ATP (**Supplementary Fig. 5b**). Thus, the docking interaction itself is not sufficient to induce phosphoacceptor binding to the p38α-2P active site.

To investigate the direct interaction between the phosphoacceptor residues of the substrate and the active site of p38α-2P, we designed the 334 peptide, which consists of a 17-aa sequence centered at phospho acceptor Thr334 (**Fig. 1b**). In the absence of the ATP analog, the 334 peptide did not induce any spectral changes in p38α-2P, even when added in ten-fold molar excess (**Supplementary Fig. 5c**). In contrast, the P+1-site methyl resonances of p38α-2P exhibited CSPs and reduction of signal intensity only in the presence of the ATP analog (**Supplementary Fig. 5d**), a characteristic that was also present with ATP (**Supplementary Fig. 5e**). In addition, in titration of p38α-2P against the 334 peptide, we observed binding-induced line-broadening only in the presence of the ATP analog (**Supplementary Fig. 5f,g**). These results clearly show that the phosphoacceptor binds to the catalytic site only when ATP is loaded onto p38α-2P.

It should be noted that there were several residues outside the P+1 site that exhibited CSPs upon 334D-peptide titration that differed depending on ATP-analog presence (**Fig. 5a**). We found that binding of the ATP analog (**Fig. 2a**) and the 334D peptide (**Fig. 4a**) to the apo–p38α-2P induced similar CSPs of the residues in the allosteric site, thus offsetting the CSPs induced by the 334D peptide to ATP-loaded p38α-2P (**Fig. 4b**). In contrast, some residues showed larger CSPs in the presence of the ATP analog. Some of these residues (for example, Leu238 and Leu285) were located between the docking site and the P+1 site in the p38α structure; thus, the enhanced CSPs in the presence of the ATP analog might also reflect the phosphoacceptor binding to the P+1 site.

Docking-enhanced kinase-reaction steps of p38α-2P

The finding that the docking interaction does not guarantee binding of the phosphoacceptor residues to the p38α-2P active site also implied that the role of the docking interaction may be more complicated. Therefore, to investigate whether the docking interaction exerts allosteric effects on the p38α-2P active site, we titrated a D peptide, which contains only the docking sequence of MK2, against ILV methyl–labeled p38α-2P in the presence of the ATP analog (**Fig. 1b**). Interestingly, we observed CSPs for both the methyl resonances of the docking site and those of Val89 in the ATP-binding site and Ile259 near the P+1 site of p38α-2P (**Supplementary Fig. 6**), each of which is distant from the docking site of p38α-2P (**Fig. 1a**). Thus, these CSPs would reflect allosteric structural modifications to the active site induced by the D-peptide binding.

We determined the binding affinities of p38α-2P to ATP and to the ATP analog in the presence or absence of the D peptide. We determined the affinity for the ATP analog by measuring the dose-dependent decrease in the intensity of the unbound-state Ile84 signal in the ATP-binding site of p38α-2P (**Fig. 6a** and **Supplementary Fig. 7a**). We observed substantial enhancement of the affinity of p38α-2P for the ATP analog upon addition of the D peptide (**Table 1**). The affinity enhancement with the D peptide was more prominent for ATP (**Table 1** and **Supplementary Fig. 7b**).

We also investigated the allosteric effect in phosphoacceptor binding to the P+1 site of p38α-2P by determining the affinity of ATP-loaded p38α-2P for the 334 peptide. The dissociation constant decreased from 80 μM to 37 μM when the D peptide was present (**Fig. 6b**, **Table 1** and **Supplementary Fig. 7c**). Furthermore, the k_{cat} for phosphorylation of the 334 peptide by p38α-2P also increased upon addition of the D peptide (**Fig. 6c**, **Table 1** and **Supplementary Fig. 7d**).

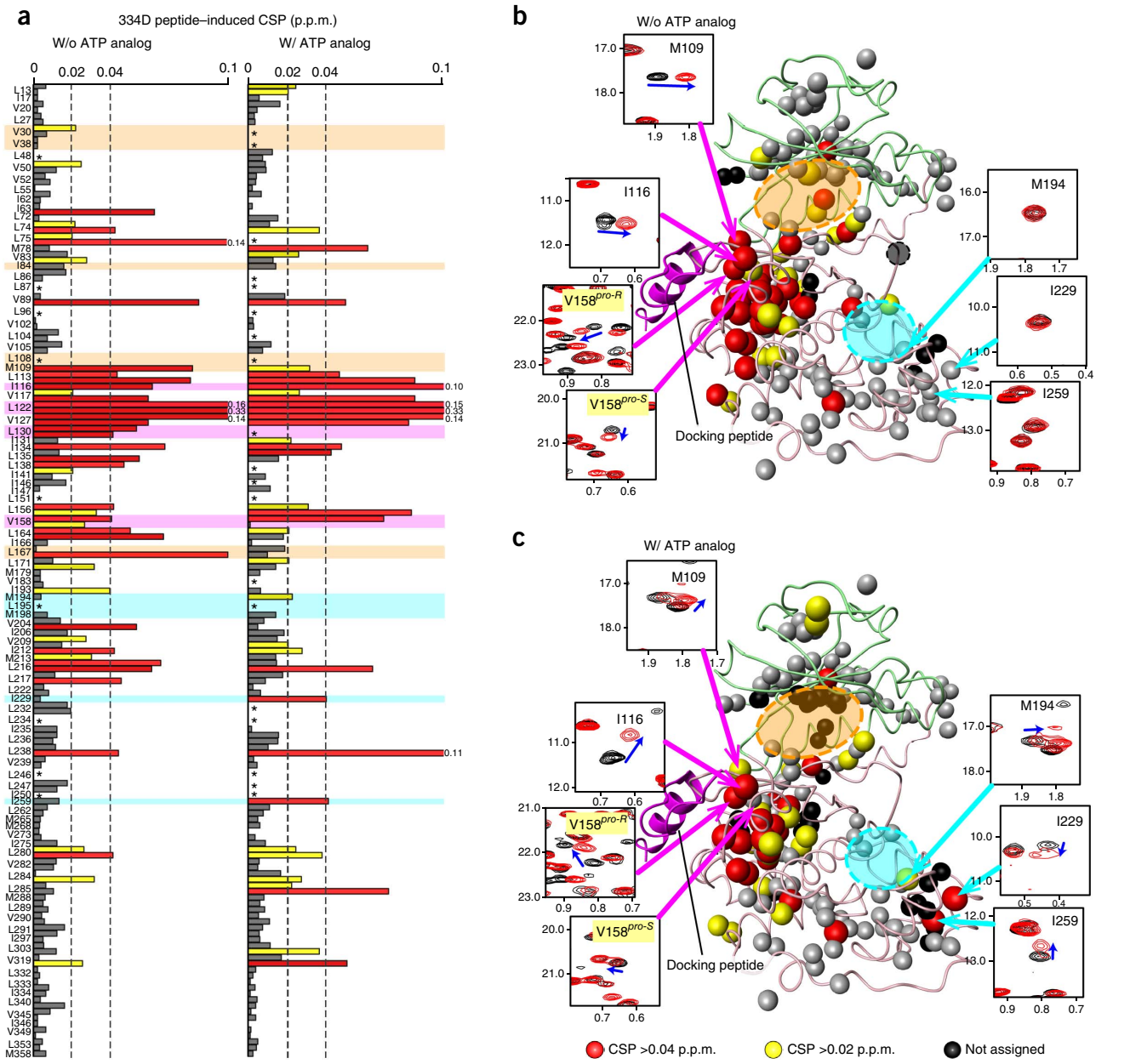

Figure 5 Site-resolved analyses of substrate binding to p38α-2P. (**a**) Bar graphs showing the methyl CSPs induced by 334D-peptide binding to p38α-2P in the absence (left) and presence (right) of the ATP analog. The residues in the ATP-binding, docking and P+1 sites are shaded in orange, magenta and cyan, respectively. Unassigned methyl sites are indicated by asterisks. CSP values larger than 0.1 p.p.m. are indicated. The CSPs at 0.02 p.p.m. and 0.04 p.p.m. are indicated by dashed gray lines. For leucine and valine, the values for δ1/γ1 are shown above the values for δ2/γ2. (**b**,**c**) Mapping of the CSPs induced by 334D-peptide binding on the crystal structure of p38α (PDB 2OKR[29]) without (**b**) and with (**c**) the ATP analog. The overlays of the ^{1}H-^{13}C spectral regions of selected methyl resonances of the hinge region (Met109), the docking sites (Ile116 and Val158) and the P+1 site (Met194, Ile229 and Ile259) are also indicated. ILVM-methyl groups that exhibited CSPs above 0.04 p.p.m. or 0.02 p.p.m. are represented as red and yellow spheres, respectively. Black spheres in **c** represent methyl groups with unassigned resonances in the 334D peptide–bound and/or the ATP analog–loaded p38α-2P. The ATP-binding and P+1 sites are indicated by orange and cyan ovals, respectively.

These results indicate that the docking interaction allosterically enhances the p38α-2P catalytic steps.

Although the high-affinity substrate MK2 forms a stable complex with p38α-2P, regardless of whether ATP is loaded on p38α-2P, other p38α substrates, such as myocyte enhancer factor 2A (MEF2A), have weaker docking affinities. For these substrates, ATP binding would occur before substrate docking. Thus, we also considered the case in which ATP is preloaded on p38α-2P. The titration of docking fragments from MEF2A and MK2 to p38α-2P in the absence or presence of the ATP analog revealed that preloading the ATP analog to p38α-2P considerably enhanced the affinity of the MEF2A docking sequence (**Supplementary Fig. 8a–d** and **Supplementary Table 1**), whereas the change in MK2 docking-sequence affinity was less substantial (**Supplementary Fig. 8e**,**f** and **Supplementary Table 1**). Thus, ATP binding and the docking interaction are mutually cooperative, and ATP preloading may contribute to specificity for substrates that dock more weakly.

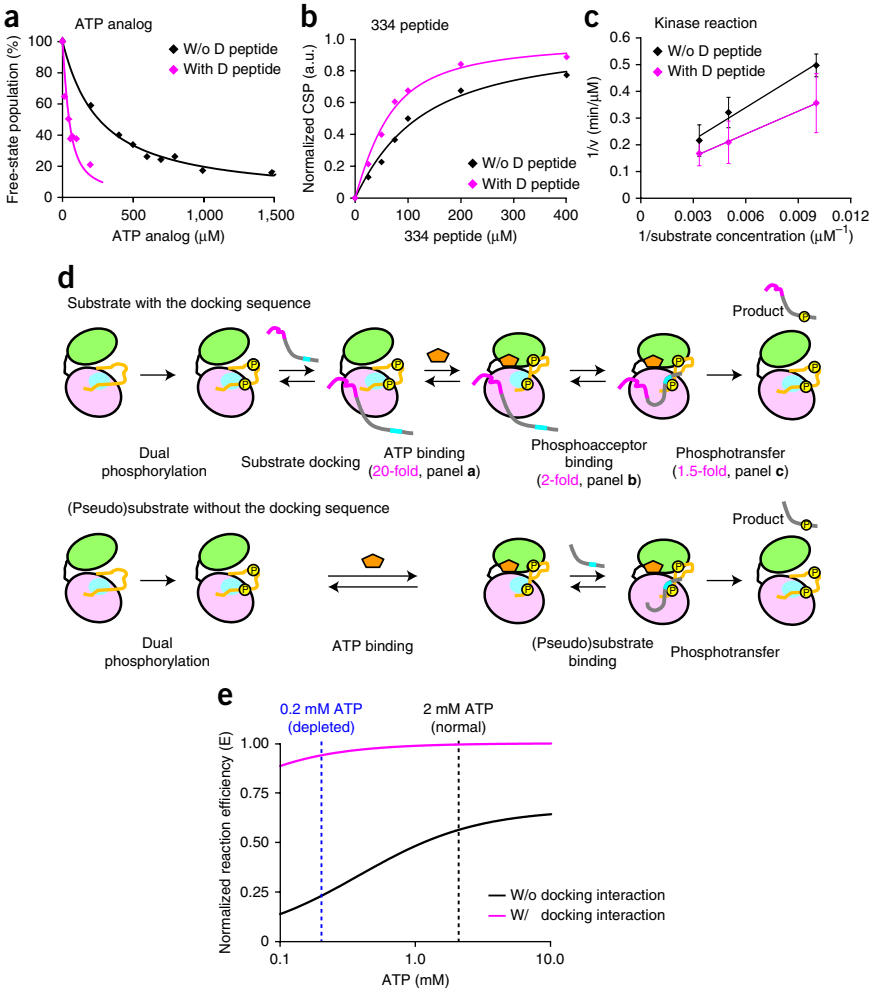

Figure 6 Allosteric positive modifications of p38α-2P kinase-reaction steps by the docking interaction. (**a**) ATP-unbound population of p38α-2P. (**b**) 334 peptide concentration–dependent, normalized CSPs of Ile259 resonances. a.u., arbitrary units. (**c**) Lineweaver-Burk plots of the phosphorylation of the 334 peptide by p38α-2P. Black and magenta lines in **a**–**c** represent data with and without the D peptide, respectively. For **a** and **b**, data representative of two independent experiments are shown. For **c**, error bars indicate the fitting errors of reaction velocities in independent experiments ($n = 3$). Experimental details are in Online Methods. (**d**) Schematic representation of p38α-2P kinase reaction process. As the initial step of activation, p38α is dually phosphorylated by the upstream MAPKKs (left). For genuine p38α substrates containing the docking sequence (top), p38α-2P recognizes the substrate via the docking interaction, binds ATP and then binds to the phosphoacceptor site of the substrate to lead to substrate phosphorylation. The docking-induced enhancements of the affinities and kinetics, in comparison to the (pseudo)substrate without the docking sequence (bottom) are indicated. Although omitted for clarification, ATP might bind before substrate docking. In that case, the affinities of the docking fragments to p38α-2P are enhanced by the ATP preloading (**Supplementary Table 1**). (**e**) ATP concentration dependence of the normalized reaction efficiencies (E) with (magenta) and without (black) formation of the docking interaction (details in Online Methods). ATP concentrations under the normal and the depleted conditions are indicated by the black and blue dashed lines, respectively.

DISCUSSION

Phosphorylation- and ATP-induced active conformation of p38α

In the previously reported crystal structures of dually phosphorylated MAPKs, both open and closed conformations have been observed[17–19,35]. Although it has been suggested that dual phosphorylation itself is sufficient to induce the conformational transition of ERK2, this notion is not consistent with the recent structures of ATP-unbound, dually phosphorylated p38α (refs. 19,35). In this study, we demonstrated that both dual phosphorylation and ATP binding are required to attain the active conformation of p38α-2P in solution (**Figs. 2** and **3** and **Supplementary Fig. 2**). This apparent difference in the requirement of ATP loading for the activating conformational transition may be due to different equilibria between the active and inactive conformations among MAPKs, or it may simply reflect the different crystallization conditions. Nevertheless, our NMR analyses clearly indicate that both dual phosphorylation and subsequent ATP loading are required for the full activation of p38α.

Table 1 Enhancements of substrate-phosphorylation steps of p38α-2P by the docking interaction

	Without D peptide	With D peptide	Enhancement ratio
K_d, ATP analog (μM)	209 ± 45[a]	17 ± 6.2[a]	12.3
K_d, ATP (μM)	381 ± 81[b]	13 ± 4.6[b]	29.3
K_d, 334 peptide (μM)	80 ± 13.0[a]	37 ± 1.5[a]	2.2
k_{cat} (/s)	17 ± 1.8[b]	24 ± 4.7[b]	1.4
K_m (μM)	420 ± 53[b]	410 ± 120[b]	1

[a]Difference between two individual experiments. [b]S.d. estimated from fitting errors.

Phosphoacceptor binding to p38α-2P requires ATP preloading

The NMR titration experiments of the 334D peptide against p38α-2P and separately observed docking and phosphoacceptor interactions clearly demonstrated that the phosphoacceptor residue binds to the P+1 site only when ATP is loaded on p38α-2P, whereas the docking interaction is spontaneous and does not require ATP loading (**Fig. 5b**,**c**). ATP binding to p38α-2P seems to be central for induction of the active conformation of the P+1 site because it enhances the interaction between the N and C lobes via the activation loop, which directly precedes the P+1 site in the amino acid sequence. ATP binding before phosphoacceptor binding seems to be structurally preferable because the ATP-binding site is located deep in the cleft between the N and C lobes, whereas the P+1 site is located outside the ATP-binding pocket. Thus, a random or inverted order may interfere with the ATP loading on p38α-2P and may prevent efficient phosphotransfer.

Kinase-reaction steps optimized by the docking interaction

We found that binding of the MK2 docking sequence to p38α-2P positively regulates each individual step in the kinase reaction: ATP loading, phosphoacceptor binding and the subsequent phosphotransfer reaction (**Fig. 6**). The affinity of p38α-2P for ATP also increased more than one order of magnitude in the presence of docking fragments derived from other p38α substrates, MEF2A and ATF2

(data not shown). Thus, the enhancement of the kinase reaction from formation of docking interactions with physiological substrates seems to be a conserved characteristic of p38α. The DEF motif, another type of docking sequence identified in many ERK1/2 substrates and consisting of a consensus sequence of FXFP[36], however, is beyond the scope of this study. Dalby and co-workers reported that the deletion of the N-terminal docking sequence of the transcription factor Ets-1 does not influence the k_{cat} of ERK2 (ref. 37); however, Ets-1 has a SAM domain that binds the FXFP site in addition to the N-terminal docking sequence. Veglia and co-workers reported that binding of either AMP-PNP or a phosphoacceptor peptide, kemptide, allosterically enhances subsequent binding of the other to the active site of protein kinase A for efficient substrate phosphorylation[38]. Our findings are distinct from the former study, showing the collaborative interplay between the kinase reaction and the docking interaction, the latter of which occurs outside the active site and represents a key element for specific substrate recognition. Thus, the allosteric enhancement of the kinase reaction by the docking interaction, shown here, couples specific substrate recognition to efficient phosphorylation, thereby providing a rationale for the strict selectivity of the MAPK pathway in the cellular context.

Biological importance of the elucidated mechanism

In the intracellular environment, many macromolecules such as proteins and nucleic acids exist at concentrations up to 300 mg/ml (ref. 39). Under such dense conditions, random collisions and nonspecific interactions between the macromolecules are expected to be common. Even under such chaotic conditions, biomolecules use multiple specific interactions and reactions to maintain cellular homeostasis and environmental responsiveness. The p38α MAPK cascade is a well-known representative of this strictly controlled signal-transduction pathway. The fine-tuned coupling between the enzymatic reaction and the specific docking interaction, shown here, may maximize the reaction efficiency for a substrate that has both the docking sequence and phosphoacceptor residues in the same polypeptide chain (**Fig. 6d**). We found that the docking interaction induces enhanced affinity for the substrate phosphoacceptor site and for ATP, corresponding to a free-energy gain of −0.4 kcal/mol and −1.8 kcal/mol, respectively. Thus, in total, the docking interaction contributes −2.2 kcal/mol energetic gain, favoring formation of the functional trimeric complex. Although the energetic gain for phosphoacceptor binding is less than that for ATP binding, the stabilization of both elements is required to enhance the formation of the functional trimeric p38α-2P–ATP–phosphoacceptor complex. In addition, the docking interaction enhanced k_{cat}. Therefore, the kinase activity of p38α toward nonspecific targets or pseudosubstrates without a docking sequence, both of which would be abundant in the cell given the simple consensus phosphoacceptor motif of MAPKs, is maintained at a very low level to avoid undesired phosphorylations and to conserve the cellular energy source, ATP (**Fig. 6d**). The mechanism diverts the specific p38α pathway, which relies on the docking interaction, from other unwanted random events so that it may appropriately integrate environmental inputs to evoke the necessary cellular responses.

Aberrant activation of protein kinases can result in fatal diseases such as cancer[40,41]. Thus, many kinases have regulatory domains that enable specific activation by certain signals and suppress activity when it is not necessary[21]. MAPKs, however, are composed of only a catalytic domain and therefore require another regulatory mechanism. The modulation of kinase activity by the docking interaction may fulfill this need. Allosteric regulation by the docking interaction seems to be reasonable, considering that p38α is the molecular hub in the MAPK cascade and must interact with several upstream and downstream molecules that belong to the same signaling cascade. Regulatory domains often exhibit very precise selectivity to certain molecules, and they might be too selective to act as molecular hubs. Thus, the docking interaction seems to provide a good balance between the requirements for both specificity and robustness of the MAPK signal. For some authentic p38α substrates lacking any docking sequences, another mechanism, such as subcellular colocalization, may operate to ensure efficient phosphorylation *in vivo*[6].

One of the most intriguing findings in this study is the affinity enhancement of p38α-2P for ATP by the docking interaction (**Fig. 6a** and **Supplementary Fig. 7a**,**b**). Most protein kinases have an apparent Michaelis constant for ATP of less than 50 μM (refs. 42,43), and such kinetics may have been evolutionarily optimized for kinases to work properly in cellular environments. The affinity of p38α-2P for ATP in the absence of the docking interaction (430 μM) is atypically weak. Although cells maintain the homeostatic ATP concentration at 1–2 mM under normal conditions, intracellular ATP concentrations can drop in certain physiological conditions that require p38α activation. For example, in the ischemic heart, the ATP concentration can be as low as 20% of the normal level[44]. Additionally, ATP concentration reportedly drops in response to UV exposure and cellular senescence[45]. Even under these ATP-depleted conditions, p38α is required to transfer stress signals[46]. The enhancement of the ATP binding affinity by the docking interaction may contribute to p38α function during stress, as shown in the simulated ATP-concentration dependence of the substrate phosphorylation efficiency by p38α (**Fig. 6e**). Thus, the allosteric regulation of p38α-2P by the docking interaction seems to be physiologically important, especially in stress-response signaling.

Although previous studies have used NMR to investigate the function and interactions of p38α (refs. 47–49), to our knowledge, our study is the first to clarify and quantify the allosteric enhancement of p38α enzymatic activity by the docking interaction. We emphasize that the observations presented here are based on firm experimental evidence using the dually phosphorylated, enzymatically active p38α. In addition, the advantage of solution NMR in providing structural information under nearly physiological conditions was crucial to revealing the structural basis for allosteric regulation.

We have shown that phosphoacceptor binding to the active site of p38α-2P requires ATP binding and that the docking interaction alone is not sufficient for the phosphoacceptor residue to bind to the active site of p38α-2P. Furthermore, the docking interaction allosterically enhances p38α-2P enzymatic function. Such regulatory mechanisms may help p38α effectively phosphorylate its specific substrates, even under low cellular ATP concentrations, while avoiding the nonspecific phosphorylation of random kinase substrates in the cell.

Given that the docking interaction is a conserved characteristic of the interactions between MAPKs and their partners, the roles of the docking interactions in other MAPKs must also be considered. In addition, there are many other examples in which the specific interactions between enzymes and substrates are distant from the catalytic cores[21]. Although it is clear that these interactions contribute to maximizing the encounter rate between the enzymes and their substrates, the possible contribution of an allosteric enhancement should also be considered.

METHODS

Methods and any associated references are available in the online version of the paper.

Accession codes. Methyl resonance assignments have been deposited in the Biological Magnetic Resonance Data Bank under accession codes 19930 (nonphosphorylated apo-p38α), 19934 (apo–p38α-2P), 19935 (p38α-2P in ATP analog–bound state), 19936 (p38α-2P in 334D peptide–bound state) and 19937 (p38α-2P in both ATP analog– and substrate-bound states).

Note: Any Supplementary Information and Source Data files are available in the online version of the paper.

ACKNOWLEDGMENTS

We would like to thank H. Hanzawa (Daiichi Sankyo Co.) for providing the expression plasmid for p38α. We are also indebted to N. Goshima (Japanese National Institute of Advanced Industrial Science and Technology) for providing cDNA clones for the phosphatases PPM1A and HePTP. This work was funded by grants from the Japan New Energy and Industrial Technology Development Organization (NEDO). Funding was also provided by Grants-in-Aid for Scientific Research on Innovative Areas (25121743 to K.T.) from the Japanese Ministry of Education, Culture, Sports, Science and Technology (MEXT) and Japan Society for the Promotion of Science (JSPS).

AUTHOR CONTRIBUTIONS

Y.T., K.T., H.T. and I.S. conceived the project. Y.T. performed the experiments. Y.T., K.T., H.T. and I.S. wrote the manuscript.

COMPETING FINANCIAL INTERESTS

The authors declare no competing financial interests.

1. Raman, M., Chen, W. & Cobb, M.H. Differential regulation and properties of MAPKs. *Oncogene* **26**, 3100–3112 (2007).
2. Avruch, J. MAP kinase pathways: the first twenty years. *Biochim. Biophys. Acta* **1773**, 1150–1160 (2007).
3. Cargnello, M. & Roux, P.P. Activation and function of the MAPKs and their substrates, the MAPK-activated protein kinases. *Microbiol. Mol. Biol. Rev.* **75**, 50–83 (2011).
4. Plotnikov, A., Zehorai, E., Procaccia, S. & Seger, R. The MAPK cascades: signaling components, nuclear roles and mechanisms of nuclear translocation. *Biochim. Biophys. Acta* **1813**, 1619–1633 (2011).
5. Marshall, C.J. Specificity of receptor tyrosine kinase signaling: transient versus sustained extracellular signal-regulated kinase activation. *Cell* **80**, 179–185 (1995).
6. Cuadrado, A. & Nebreda, A.R. Mechanisms and functions of p38 MAPK signalling. *Biochem. J.* **429**, 403–417 (2010).
7. Schindler, J.F., Monahan, J.B. & Smith, W.G. p38 pathway kinases as anti-inflammatory drug targets. *J. Dent. Res.* **86**, 800–811 (2007).
8. Dodeller, F. & Schulze-Koops, H. The p38 mitogen-activated protein kinase signaling cascade in CD4 T cells. *Arthritis Res. Ther.* **8**, 205 (2006).
9. Johnson, G.L. & Lapadat, R. Mitogen-activated protein kinase pathways mediated by ERK, JNK, and p38 protein kinases. *Science* **298**, 1911–1912 (2002).
10. Anderson, N.G., Maller, J.L., Tonks, N.K. & Sturgill, T.W. Requirement for integration of signals from two distinct phosphorylation pathways for activation of MAP kinase. *Nature* **343**, 651–653 (1990).
11. Zhang, Y.Y., Mei, Z.Q., Wu, J.W. & Wang, Z.X. Enzymatic activity and substrate specificity of mitogen-activated protein kinase p38α in different phosphorylation states. *J. Biol. Chem.* **283**, 26591–26601 (2008).
12. Keyse, S.M. Protein phosphatases and the regulation of mitogen-activated protein kinase signalling. *Curr. Opin. Cell Biol.* **12**, 186–192 (2000).
13. Goldsmith, E.J., Cobb, M.H. & Chang, C.I. Structure of MAPKs. *Methods Mol. Biol.* **250**, 127–144 (2004).
14. Wang, Z. *et al.* The structure of mitogen-activated protein kinase p38 at 2.1-A resolution. *Proc. Natl. Acad. Sci. USA* **94**, 2327–2332 (1997).
15. Wilson, K.P. *et al.* Crystal structure of p38 mitogen-activated protein kinase. *J. Biol. Chem.* **271**, 27696–27700 (1996).
16. Zhang, F., Strand, A., Robbins, D., Cobb, M. & Goldsmith, E. Atomic structure of the MAP kinase ERK2 at 2.3 A resolution. *Nature* **367**, 704–711 (1994).
17. Bellon, S., Fitzgibbon, M.J., Fox, T., Hsiao, H.M. & Wilson, K.P. The structure of phosphorylated p38γ is monomeric and reveals a conserved activation-loop conformation. *Structure* **7**, 1057–1065 (1999).
18. Canagarajah, B.J., Khokhlatchev, A., Cobb, M.H. & Goldsmith, E.J. Activation mechanism of the MAP kinase ERK2 by dual phosphorylation. *Cell* **90**, 859–869 (1997).
19. Zhang, Y.Y., Wu, J.W. & Wang, Z.X. Mitogen-activated protein kinase (MAPK) phosphatase 3-mediated cross-talk between MAPKs ERK2 and p38α. *J. Biol. Chem.* **286**, 16150–16162 (2011).
20. Weston, C.R., Lambright, D.G. & Davis, R.J. Signal transduction. MAP kinase signaling specificity. *Science* **296**, 2345–2347 (2002).
21. Ubersax, J.A. & Ferrell, J.E. Mechanisms of specificity in protein phosphorylation. *Nat. Rev. Mol. Cell Biol.* **8**, 530–541 (2007).
22. Tanoue, T. & Nishida, E. Docking interactions in the mitogen-activated protein kinase cascades. *Pharmacol. Ther.* **93**, 193–202 (2002).
23. Tanoue, T., Adachi, M., Moriguchi, T. & Nishida, E. A conserved docking motif in MAP kinases common to substrates, activators and regulators. *Nat. Cell Biol.* **2**, 110–116 (2000).
24. Gupta, S., Campbell, D., Derijard, B. & Davis, R.J. Transcription factor ATF2 regulation by the JNK signal transduction pathway. *Science* **267**, 389–393 (1995).
25. Kallunki, T. *et al.* JNK2 contains a specificity-determining region responsible for efficient c-Jun binding and phosphorylation. *Genes Dev.* **8**, 2996–3007 (1994).
26. Yang, S.-H., Galanis, A. & Sharrocks, A.D. Targeting of p38 mitogen-activated protein kinases to MEF2 transcription factors. *Mol. Cell. Biol.* **19**, 4028–4038 (1999).
27. Lukas, S.M. *et al.* Catalysis and function of the p38α-MK2a signaling complex. *Biochemistry* **43**, 9950–9960 (2004).
28. Chang, C.I., Xu, B.E., Akella, R., Cobb, M.H. & Goldsmith, E.J. Crystal structures of MAP kinase p38 complexed to the docking sites on its nuclear substrate MEF2A and activator MKK3b. *Mol. Cell* **9**, 1241–1249 (2002).
29. ter Haar, E., Prabhakar, P., Prabakhar, P., Liu, X. & Lepre, C. Crystal structure of the p38α-MAPKAP kinase 2 heterodimer. *J. Biol. Chem.* **282**, 9733–9739 (2007).
30. Tanoue, T., Maeda, R., Adachi, M. & Nishida, E. Identification of a docking groove on ERK and p38 MAP kinases that regulates the specificity of docking interactions. *EMBO J.* **20**, 466–479 (2001).
31. Reményi, A., Good, M.C., Bhattacharyya, R.P. & Lim, W.A. The role of docking interactions in mediating signaling input, output, and discrimination in the yeast MAPK network. *Mol. Cell* **20**, 951–962 (2005).
32. Songyang, Z. *et al.* A structural basis for substrate specificities of protein Ser/Thr kinases: primary sequence preference of casein kinases I and II, NIMA, phosphorylase kinase, calmodulin-dependent kinase II, CDK5, and Erk1. *Mol. Cell. Biol.* **16**, 6486–6493 (1996).
33. White, A., Pargellis, C.A., Studts, J.M., Werneburg, B.G. & Farmer, B.T. Molecular basis of MAPK-activated protein kinase 2:p38 assembly. *Proc. Natl. Acad. Sci. USA* **104**, 6353–6358 (2007).
34. Szafranska, A.E. & Dalby, K.N. Kinetic mechanism for p38 MAP kinase α. *FEBS J.* **272**, 4631–4645 (2005).
35. Akella, R., Min, X., Wu, Q., Gardner, K.H. & Goldsmith, E.J. The third conformation of p38α MAP kinase observed in phosphorylated p38α and in solution. *Structure* **18**, 1571–1578 (2010).
36. Jacobs, D., Glossip, D., Xing, H., Muslin, A.J. & Kornfeld, K. Multiple docking sites on substrate proteins form a modular system that mediates recognition by ERK MAP kinase. *Genes Dev.* **13**, 163–175 (1999).
37. Lee, S. *et al.* A model of a MAPKsubstrate complex in an active conformation: a computational and experimental approach. *PLoS ONE* **6**, e18594 (2011).
38. Masterson, L.R., Mascioni, A., Traaseth, N.J., Taylor, S.S. & Veglia, G. Allosteric cooperativity in protein kinase A. *Proc. Natl. Acad. Sci. USA* **105**, 506–511 (2008).
39. Zimmerman, S.B. & Trach, S.O. Estimation of macromolecule concentrations and excluded volume effects for the cytoplasm of *Escherichia coli*. *J. Mol. Biol.* **222**, 599–620 (1991).
40. Lugo, T.G., Pendergast, A.M., Muller, A.J. & Witte, O.N. Tyrosine kinase activity and transformation potency of bcr-abl oncogene products. *Science* **247**, 1079–1082 (1990).
41. Heisterkamp, N. *et al.* Acute leukaemia in *bcr/abl* transgenic mice. *Nature* **344**, 251–253 (1990).
42. Dennis, P.B. *et al.* Mammalian TOR: a homeostatic ATP sensor. *Science* **294**, 1102–1105 (2001).
43. Knight, Z.A. & Shokat, K.M. Features of selective kinase inhibitors. *Chem. Biol.* **12**, 621–637 (2005).
44. Steenbergen, C., Murphy, E., Watts, J.A. & London, R.E. Correlation between cytosolic free calcium, contracture, ATP, and irreversible ischemic injury in perfused rat heart. *Circ. Res.* **66**, 135–146 (1990).
45. Schütt, F., Aretz, S., Auffarth, G.U. & Kopitz, J. Moderately reduced ATP levels promote oxidative stress and debilitate autophagic and phagocytic capacities in human RPE cells. *Invest. Ophthalmol. Vis. Sci.* **53**, 5354–5361 (2012).
46. Kumphune, S., Chattipakorn, S. & Chattipakorn, N. Role of p38 inhibition in cardiac ischemia/reperfusion injury. *Eur. J. Clin. Pharmacol.* **68**, 513–524 (2012).
47. Nielsen, G. & Schwalbe, H. NMR spectroscopic investigations of the activated p38α mitogen-activated protein kinase. *ChemBioChem* **12**, 2599–2607 (2011).
48. Francis, D.M. *et al.* Structural basis of p38α regulation by hematopoietic tyrosine phosphatase. *Nat. Chem. Biol.* **7**, 916–924 (2011).
49. Piserchio, A. *et al.* Docking interactions of hematopoietic tyrosine phosphatase with MAP kinases ERK2 and p38α. *Biochemistry* **51**, 8047–8049 (2012).
50. Arnold, K., Bordoli, L., Kopp, J. & Schwede, T. The SWISS-MODEL workspace: a web-based environment for protein structure homology modelling. *Bioinformatics* **22**, 195–201 (2006).
51. Wang, Z. *et al.* Structural basis of inhibitor selectivity in MAP kinases. *Structure* **6**, 1117–1128 (1998).

ONLINE METHODS

Preparation of unphosphorylated p38α. The pET15b vector for the expression of human p38α (aa 2–360) with an N-terminal hexahistidine (His_6) tag was a kind gift from H. Hanzawa (Daiichi Sankyo Co.). The *Escherichia coli* BL21 (DE3) transformed with the plasmid was grown in 10 mL of Luria-Bertani (LB) medium containing 100 mg/mL ampicillin, at 37 °C overnight. The cells were further inoculated into 1 l of D_2O-based ampicillin-M9 medium supplemented with D-[$^2H_7$/$^{13}C_6$]glucose and $^{15}NH_4Cl$ as the sole carbon and nitrogen sources, respectively. When the culture attained an optical density at a wavelength of 600 nm (OD_{600}) of 0.6, 0.5 mM isopropyl-β-D-thiogalactopyranoside (IPTG) was added to induce protein expression. The culture was further incubated at 16 °C for 16 h. For selective $^{13}CH_3$ labeling of the isoleucine (δ1), leucine, valine and methionine methyl groups in a $^2H/^{12}C$ background (so-called ILVM-methyl labeling[52,53]), 70 mg/L of [methyl-^{13}C, 3,3-$^2H_2$]α-ketobutyric acid, 100 mg/L of [3-methyl-^{13}C, 3,4,4,4-$^2H_4$]α-ketoisovaleric acid and 50 mg/L of L-[methyl-^{13}C]methionine were supplemented into the medium, 30 min before the addition of IPTG. The p38α was purified from the supernatant of the cell lysate by two column-chromatography steps, including nickel affinity and SEC. The cell lysate was applied to an Ni-NTA agarose (Qiagen) column equilibrated with a buffer consisting of 20 mM Tris-HCl, pH 8.0, 500 mM NaCl, 2 mM dithiothreitol (DTT), 10 mM imidazole and 0.6% (w/v) CHAPS. After thorough washing of the column with the equilibration buffer, p38α was eluted with the same buffer but containing 250 mM imidazole. The eluate was further purified by SEC, with a HiLoad Superdex 200 prep-grade column (GE Healthcare), which was equilibrated with a buffer containing 50 mM NaPi, pH 6.8, 150 mM NaCl and 3 mM DTT. The eluate fraction was buffer-exchanged into 25 mM Tris-HCl, pH 7.5, with 150 mM NaCl and 5 mM DTT and stored at −30 °C until use.

Preparation of the constitutively active MAPKK6. The cDNA clone of human MAPKK6 (MKK6) was purchased from Toyobo. MKK6 (aa 1–334) was subcloned into the pGEX-5X-3 vector with an N-terminal glutathione S-transferase (GST) tag followed by a factor Xa cleavage site. The constitutively active S207D T211D MKK6 mutant ($MKK6^{DD}$) was constructed with a QuikChange Mutagenesis Kit (Agilent Technologies). BL21 (DE3) cells transformed with the plasmid were grown in LB medium. When the culture attained an OD_{600} of 0.6, 0.5 mM IPTG was added to induce protein expression. The culture was then incubated at 16 °C for 20 h. The $MKK6^{DD}$ protein was purified by GST-affinity chromatography. Briefly, the cells, resuspended in 50 mL of buffer (10 mM Tris-HCl, pH 8.0, 100 mM NaCl, 1 mM EDTA and 10% (w/v) glycerol), were lysed by sonication. Triton X-100 and DTT were added to final concentrations of 1% (w/v) and 2 mM, respectively. The lysate was incubated at 4 °C for 30 min with rotation. The supernatant was applied to a glutathione Sepharose 4B column (GE Healthcare). After the column was thoroughly washed, $MKK6^{DD}$ was eluted with buffer containing 25 mM Tris-HCl, pH 7.4, 150 mM NaCl, 2 mM DTT and 50 mM reduced glutathione. The eluate was buffer-exchanged by dialysis against 1 l of storage buffer, containing 25 mM Tris-HCl, pH 7.5, 150 mM NaCl, 2 mM DTT and 10% (w/v) glycerol. The resulting stock was stored on ice, and its activity was retained for at least six months.

Preparation of the p38α substrate, MK2. The full-length cDNA clone of human MK2 was purchased from Toyobo. From the MK2 cDNA, four fragments corresponding to aa 47–400, 326–400 (334D peptide), 326–342 (334 peptide) and 369–400 (D peptide) were amplified by polymerase chain reaction (PCR) (**Fig. 1b**). The longer MK2 fragment (aa 47–400) was ligated into the pET15b vector with an N-terminal His_6 tag. The smaller MK2 fragments were ligated into the pET28a vector with an N-terminal GB1 tag followed by a human rhinovirus 3C (HRV3C) cleavage site and a C-terminal His_6 tag. These plasmids were transformed into BL21 (DE3) for protein expression. The bacterial culture for the D peptide was grown in LB medium, whereas cultures for MK2, the 334D peptide and the 334 peptide were grown in M9 medium. When the cultures reached an OD_{600} of 0.6, the medium was supplemented with 1 mM IPTG, and the cultures were then incubated at 25 °C for 12 h. The longer MK2 fragment was purified with a four-step column-chromatography procedure according to the previously reported protocol[54], with minor modifications. The 334D, 334 and D peptides were purified by nickel-affinity chromatography. The GB1 tag was removed from the D peptide by HRV3C protease and then separated from HRV3C and GB1 by nickel-affinity chromatography.

Preparation of dually phosphorylated p38α (p38α-2P). Unphosphorylated p38α (10 μM) was phosphorylated by a 0.014 molar equivalent of $MKK6^{DD}$, in a reaction buffer containing 50 mM Tris-HCl, pH 8.0, 100 mM NaCl, 2 mM DTT, 10 mM $MgCl_2$, 0.5 mM EDTA and 2 mM ATP, by following a previously published protocol with minor modifications[11]. The reaction was carried out at 14 °C for 48 h. The completion of the dual-phosphorylation reaction was confirmed by SDS-PAGE, with a 9% polyacrylamide gel supplemented with 30 μM of Phos-tag acrylamide[55] (**Supplementary Fig. 1a**), as well as by NMR (**Supplementary Fig. 1b–i**). p38α-2P was isolated from $MKK6^{DD}$ by nickel-affinity chromatography. The kinase activity of the prepared p38α-2P was measured by an *in vitro* kinase assay at 25 °C with MK2 as the substrate. The reaction mixture consisted of 5 μM MK2 and 0.5 μM p38α-2P, in the same buffer used for the phosphorylation of p38α by $MKK6^{DD}$. Phosphorylation of MK2 was confirmed by Phos-tag SDS-PAGE (**Supplementary Fig. 1j**). The active p38α-2P was used for further analysis.

NMR experiments. Vogtherr *et al.*[56] reported that 25% of the backbone-amide ^1H-^{15}N resonances in the unphosphorylated p38α were not observed, probably because of local conformational multiplicities, and 36% of the backbone resonances were not assigned. The unobservable/unassigned regions contain the residues in the ATP-binding site and a large part of the phosphoacceptor-binding site. Therefore, we used the methyl-TROSY technique[57] to obtain the structural information for these sites. Methyl $^1H/^{13}C$ resonances are highly sensitive in a uniformly deuterated background and thus provide high-quality NMR spectra. The ILVM-methyl moieties of p38α were selectively $^1H/^{13}C$-labeled with established protocols[58].

Uniformly $^2H/^{13}C/^{15}N$-labeled p38α-2P was concentrated to 0.1–0.4 mM in 220 μL of aqueous buffer containing 25 mM Tris-HCl, pH 7.5, 150 mM NaCl, 5 mM DTT and 10% D_2O. NMR samples of ILVM (or ILV) methyl–labeled p38α-2P were prepared in D_2O-based buffer at protein concentrations of 20 μM and 40 μM for two-dimensional (2D) experiments and 0.3 mM for three-dimensional (3D) experiments. For the analysis of p38α-2P in the presence of ATP or analogous compounds such as ADP, 5′-adenylyl imidodiphosphate (AMP-PNP), adenylyl methylenediphosphate (AMP-PCP), ATP-γS and AMP, the buffer was supplemented with 20 mM $MgCl_2$. We found that p38α-2P has intrinsic ATPase activity, and more than 50% of 1 mM ATP was hydrolyzed in 30 min at 25 °C in the presence of 20 μM p38α-2P (data not shown). To avoid chemical inhomogeneity due to ATP hydrolysis by p38α-2P, we used ADP as an ATP analog unless otherwise indicated. ADP had almost the same affinity for p38α-2P as did ATP, and the NMR spectrum of the ADP-bound p38α-2P closely matched that of the ATP-loaded p38α-2P (data not shown). The NMR spectra of p38α-2P in complex with other conventional ATP analogs, such as AMP-PNP, AMP-PCP and ATP-γS, did not fully reproduce the spectrum with ATP. Thus, we chose ADP as the most appropriate ATP analog for this study. To obtain the ATP-bound p38α-2P spectra, the experimental time was shortened with a ^1H-^{13}C SOFAST-HMQC experiment[59] and the highest-field magnet (800 MHz in ^1H frequency) equipped with a TCI cryoprobe. Experiments were conducted at a low temperature (10 °C) to minimize ATP hydrolysis. Under these conditions, the ATP hydrolysis during the experiment was suppressed to less than 10%, as confirmed by the ^1H-1D spectra before and after the SOFAST-HMQC measurement. For kinetic analyses of 334-peptide phosphorylation, a buffer consisting of 50 mM Tris-HCl, pH 8.0, 100 mM NaCl, 2 mM DTT, 0.5 mM EDTA, 10 mM $MgCl_2$ and 10% D_2O was used. All NMR spectra were measured at 600, 700 and 800 MHz ^1H frequencies on Bruker Avance spectrometers equipped with a TXI cryoprobe, a TXI room-temperature probe and a TCI cryoprobe, respectively. All NMR experiments were performed at 25 °C, except for the ^1H-^{13}C SOFAST-HMQC experiments for p38α-2P in the presence of ATP. NMR data were processed with TopSpin 2.1 (Bruker) and analyzed with CARA (http://cara.nmr-software.org/downloads/) and Sparky (http://www.cgl.ucsf.edu/home/sparky/).

In the NMR interaction analyses between p38α-2P and the substrate peptides, average CSPs of methyl ^1H-^{13}C correlations are defined as

$$\Delta\omega_{avg} = \sqrt{\Delta\omega_H^2 + \left(\frac{\Delta\omega_C^2}{5.6}\right)}$$

where $\Delta\omega_H$ and $\Delta\omega_C$ are CSPs in ^1H and ^{13}C dimensions, respectively. The scaling factor 5.6 is used in the ^{13}C dimension, which is the ratio of the chemical-shift deviations of methyl ^{13}C and ^1H nuclei deposited in the Biological Magnetic Resonance Data Bank.

doi:10.1038/nsmb.2861

NMR resonance assignments of p38α. Backbone resonance assignments of p38α were performed with standard TROSY-type triple-resonance NMR spectra, including HNCA, HN(CO)CA, HNCACB, HN(CO)CACB, HNCO and HN(CA)CO. For the assignments of p38α-2P in complex with the ATP analog, alanine, phenylalanine, histidine, methionine, threonine and tyrosine ^{15}N-amino acid–type selectively labeled p38α-2P were also used. The completeness percentage of the assignments for unphosphorylated p38α, p38α-2P and p38α-2P bound to the ATP analog were 61%, 59% and 48% of 342 nonproline residues, respectively. The completeness of the assignment for the unphosphorylated p38α was the same as that reported previously (BMRB 6468)[56]. As discussed above, incomplete assignments are mainly due to the intrinsic local dynamics of p38α.

Assignments of the ILVM-methyl resonances were performed by combining mutational analyses, *J* coupling–based triple-resonance experiments ((H)CC(CO)NH, H(CCCO)NH, and HCCH-TOCSY experiments), and an intermethyl ^{1}H-^{1}H NOE network analysis based on the crystal structures. For the ILVM-methyl resonances, assignments were achieved for 95%, 95% and 78% of all 152 methyl resonances in apo-p38α, apo-p38α-2P and the p38α-2P bound to the ATP analog, respectively. As for the isoleucine-δ1 and methionine-ε resonances, more than 90% of the resonances were assigned under all experimental conditions. These assignments provided highly sensitive site-specific information for all of the functional elements in p38α.

Preparation of the p38α-specific phosphatases PPM1A and HePTP. The cDNA clones encoding human protein phosphatase Mg^{2+}/Mn^{2+} dependent 1A (PPM1A) and hematopoietic protein tyrosine phosphatase (HePTP) were gifts from N. Goshima (AIST), and were originally from the NEDO full-length human cDNA sequencing project. The information about these clones is available in the Human Gene and Protein Database (HGPD) (http://hgpd.lifesciencedb.jp/cgi/)[60,61]. DNA fragments corresponding to amino acid residues 15–339 of PPM1A and 1–382 of HePTP were amplified by PCR. The PPM1A fragment was ligated into the pET28a vector (Merck Millipore) without a purification tag, whereas the HePTP fragment was ligated into the pET15b vector (Merck Millipore) with an N-terminal His_6 tag. Each of these plasmids was transformed into *E. coli* BL21 (DE3) cells, and the bacteria were grown in LB medium. When the cultures reached an OD_{600} of 0.6, the culture medium was supplemented with 1 mM IPTG and was incubated at 30 °C for 8 h. PPM1A was purified by cation-exchange chromatography and SEC. HePTP was purified by nickel-affinity chromatography and SEC. Dephosphorylation of p38α-2P by these phosphatases was performed with 10 μM p38α-2P in the presence of 0.01 molar equivalent of phosphatases. The reaction was performed in 50 mM MOPS, pH 7.0, 100 mM NaCl, 10 mM $MgCl_2$, 0.1 mM EDTA and 2 mM DTT, for 1 h at room temperature, by following a previously published protocol with minor modifications[11].

Competition experiment between the 334D peptide and MK2 for p38α-2P. In this competition assay, p38α-2P in solution was assayed for binding between the N-terminally GB1-fused 334D peptide (GB1-334D peptide) immobilized on IgG beads and a soluble, longer MK2 fragment (aa 47–400). All proteins or peptides were prepared in a buffer consisting of 50 mM Tris-HCl, pH 7.5, 150 mM NaCl, 2 mM DTT and 0.05% (v/v) Tween 20 (TBST buffer). A 50-μL bead volume of IgG Sepharose 6 Fast Flow (GE Healthcare) was suspended in 300 μL of the 5-μM solution of the GB1-334D peptide and incubated with gentle shaking at 4 °C for 1 h. After the beads were washed three times with 300 μL TBST buffer, they were suspended in 300 μL of the 5 μM solution of p38α-2P and incubated at 4 °C for 1 h. The beads were washed five times with 300 μL of the TBST buffer. Then the beads were suspended in 500 μL of the solution of the longer MK2 fragment, at concentrations of 0.3, 0.6 or 1.2 μM in 500 μL of the TBST buffer, and incubated at 4 °C for 1 h. GB1 was used instead of the GB1-334D peptide, as a control. For the eluate from the control experiment, the solution of the longer MK2 fragment was prepared at 5 μM. Supernatants from the bead suspension in the solution of the longer MK2 fragment were analyzed by SDS-PAGE and transferred to a PVDF membrane. Western blotting of p38α-2P was performed, with a 1:1,000 dilution of the anti-p38 mouse monoclonal antibody (Cell Signaling Technology; 9228S) as the first antibody and a 1:10,000 dilution of horseradish peroxidase (HRP)-conjugated anti-mouse IgG (Santa Cruz Biotechnology; sc-2005) as the second antibody. These antibodies have been verified by the manufacturers to recognize human p38α and mouse IgG, respectively, with validation available on the manufacturers' websites. Bound HRP conjugates were detected by chemiluminescence, derived from the oxidization of luminol catalyzed by HRP in the presence of hydrogen peroxide.

Determination of the affinity of p38α-2P for the ATP analog. The ATP analog was added to 40 μM of ILV methyl–labeled p38α-2P at 0.2, 0.4, 0.5, 0.6, 0.7, 0.8, 1.0 and 1.5 mM in the absence of the D peptide, and at 20, 40, 60, 80, 100 and 200 μM concentrations in the presence of a 1.1 equimolar amount of the D peptide (**Supplementary Fig. 7a**). The resonance from the δ1-methyl group of Ile84 in the ATP-binding site exhibited distinct chemical shifts between the ATP analog–unbound and analog-bound forms. The intensities of the resonance derived from the unbound state were fit by assuming 1:1 binding.

Determination of the affinity of p38α-2P for ATP. The affinity of p38α-2P for ATP was determined by the competition experiment with the ATP analog, with the following relationship:

$$K_{\mathrm{d}}^{\mathrm{ATP}} = K_{\mathrm{d}}^{\mathrm{ATP\,analog}} \times \frac{[\mathrm{p38\alpha^{2P}} \times \mathrm{ATP\,analog}]}{[\mathrm{p38\alpha^{2P}} \times \mathrm{ATP}]} \times \frac{[\mathrm{ATP}]^0 - [\mathrm{p38\alpha^{2P}} \times \mathrm{ATP}]}{[\mathrm{ATP\,analog}]^0 - [\mathrm{p38\alpha^{2P}} \times \mathrm{ATP\,analog}]}$$

where $[ATP]^0$ and $[ATP\ analog]^0$ are the total concentration of each compound (2.5 mM). The concentrations of p38α-2P that bound ATP ($[p38\alpha^{2P} \times ATP]$) and the ATP analog ($[p38\alpha^{2P} \times ATP\ analog]$) were estimated from the intensities of the NMR signals that have distinct chemical shifts in the ATP- and ATP analog–bound states (**Supplementary Fig. 7b**). In both the absence and presence of the D peptide, ^{1}H-^{13}C SOFAST-HMQC spectra of 20 μM ILV methyl–labeled p38α-2P were acquired in the presence of the mixture of 2.5 mM ATP and 2.5 mM ATP analog. The spectra in the presence of either 5 mM ATP or 5 mM ATP analog were used as the reference for the intensity of each state. The experiments were conducted at 10 °C to suppress ATP hydrolysis. The loss of ATP during the experiment was negligible.

Determination of the affinity of p38α-2P for the 334 peptide. 50 μM of ILV methyl–labeled p38α-2P was titrated with the 334 peptide (**Supplementary Fig. 7c**). The 334 peptide was added at 25, 50, 75, 100, 200 and 400 μM in both the absence and presence of 1.1 molar equivalent of the D peptide. The CSPs of the δ1-methyl group of Ile259, which is located near the P+1 site, were fit to a 1:1 binding model, and the dissociation constant was determined.

Determination of the kinetic constants for phosphorylation of the 334 peptide by p38α-2P. Phosphorylation of the [U-^{15}N]334 peptide by p38α-2P was confirmed by MALDI-TOF mass spectrometry with an AXIMA spectrometer (Shimadzu) (data not shown) and by the ^{1}H-^{15}N HSQC spectra before and after p38α-2P treatment (**Supplementary Fig. 7d**). Phosphorylation at Thr334 was confirmed with the T334A mutant of the 334 peptide. The time course of the phosphorylation was monitored by successive measurements of ^{1}H-^{15}N SOFAST-HMQC spectra[62] (**Supplementary Fig. 7d**). The intensity of the resonance derived from the pThr334 exhibited characteristic low field shifts in both dimensions[63]. The 334 peptide at concentrations of 100, 200 and 300 μM was phosphorylated by 10 nM of p38α-2P in the absence and presence of 10 μM D peptide. The kinetic constants were determined by the Lineweaver-Burk plot.

Calculation of normalized reaction efficiency. The normalized reaction efficiency (E) was calculated by the population of the functional trimeric p38α-2P–ATP–phosphoacceptor complex, and the catalytic rates were calculated, assuming the K_{d} and k_{cat} values in **Table 1**. Under physiological conditions, in which $[ATP]_{tot} >> [p38]_{tot}$, $[substrate]_{tot}$, E is described by the equation $E = A \times k_{cat} \times ([ATP]_{tot} / K_{\mathrm{d}}^{\mathrm{ATP}} + [ATP]_{tot})$. A is a constant, which includes p38α.

Determination of the affinities of p38α-2P for the docking fragments. The ^{1}H-^{13}C HMQC spectra of ILV methyl–labeled p38α-2P (20 μM) were measured in the presence of increasing amounts of the docking fragment derived from the substrate MEF2A (**Supplementary Fig. 8a**,**b**). The docking fragment was added to p38α at 20, 50, 100, 200, 400 and 500 μM in the absence of the ATP analog, and at 5, 10, 20, 40, 80 and 160 μM in the presence of 4 mM ATP analog (**Supplementary Fig. 8c**,**d**). The CSPs in the δ1-methyl signal of Ile116, which is located in the docking site, were fit to a 1:1 binding model, and the dissociation constant was determined.

To determine the affinity of p38α-2P for the D peptide, isothermal titration calorimetry (ITC) experiments were performed with a VP-ITC calorimeter (MicroCal) (**Supplementary Fig. 8e**,**f**). The D peptide (500 μM) was added from the syringe to p38α-2P (50 μM) in the isothermal cell by 25 injection steps, in either the absence or presence of 4 mM ATP analog. Experiments were performed at 25 °C. The dissociation constant was determined by fitting the calorimetric data to a 1:1 binding model, with Origin software.

52. Gardner, K.H., Rosen, M.K. & Kay, L.E. Global folds of highly deuterated, methyl-protonated proteins by multidimensional NMR. *Biochemistry* **36**, 1389–1401 (1997).
53. Rosen, M.K. *et al.* Selective methyl group protonation of perdeuterated proteins. *J. Mol. Biol.* **263**, 627–636 (1996).
54. Underwood, K.W. *et al.* Catalytically active MAP KAP kinase 2 structures in complex with staurosporine and ADP reveal differences with the autoinhibited enzyme. *Structure* **11**, 627–636 (2003).
55. Kinoshita, E., Takahashi, M., Takeda, H., Shiro, M. & Koike, T. Recognition of phosphate monoester dianion by an alkoxide-bridged dinuclear zinc(II) complex. *Dalton Trans.* **21**, 1189–1193 (2004).
56. Vogtherr, M. *et al.* NMR backbone assignment of the mitogen-activated protein (MAP) kinase p38. *J. Biomol. NMR* **32**, 175 (2005).
57. Tugarinov, V., Hwang, P.M., Ollerenshaw, J.E. & Kay, L.E. Cross-correlated relaxation enhanced ^{1}H-^{13}C NMR spectroscopy of methyl groups in very high molecular weight proteins and protein complexes. *J. Am. Chem. Soc.* **125**, 10420–10428 (2003).
58. Goto, N.K., Gardner, K.H., Mueller, G.A., Willis, R.C. & Kay, L.E. A robust and cost-effective method for the production of Val, Leu, Ile (δ1) methyl-protonated 15N-, 13C-, 2H-labeled proteins. *J. Biomol. NMR* **13**, 369–374 (1999).
59. Amero, C. *et al.* Fast two-dimensional NMR spectroscopy of high molecular weight protein assemblies. *J. Am. Chem. Soc.* **131**, 3448–3449 (2009).
60. Maruyama, Y. *et al.* Human Gene and Protein Database (HGPD): a novel database presenting a large quantity of experiment-based results in human proteomics. *Nucleic Acids Res.* **37**, D762–D766 (2009).
61. Maruyama, Y. *et al.* HGPD: Human Gene and Protein Database, 2012 update. *Nucleic Acids Res.* **40**, D924–D929 (2012).
62. Schanda, P., Kupce, E. & Brutscher, B. SOFAST-HMQC experiments for recording two-dimensional heteronuclear correlation spectra of proteins within a few seconds. *J. Biomol. NMR* **33**, 199–211 (2005).
63. Selenko, P. *et al. In situ* observation of protein phosphorylation by high-resolution NMR spectroscopy. *Nat. Struct. Mol. Biol.* **15**, 321–329 (2008).

doi:10.1038/nsmb.2861